analytical chemistry

Review

pubs.acs.org/ac

Nanoscale Electrochemistry Revisited

Stephen M. Oja, Yunshan Fan, Chadd M. Armstrong, Peter Defnet, and Bo Zhang*

Department of Chemistry, University of Washington, Seattle, Washington 98195-1700, United States

CONTENTS

The field of nanoscale electrochemistry has received enormous attention in the last several years with numerous exciting advancements reported in several rapidly growing areas. These are driven at least partially by the need to characterize and develop a better understanding of nanomaterials in fields such as energy, catalysis, and environmental research. The use of specially designed, multifunctional nanoelectrodes has enabled characterization and imaging of electrochemical surfaces and reactivity of materials of exceedingly small dimensions approaching single catalytic nanoparticles. A rapid growth has been seen in the use of ultramicroelectrodes (UMEs) to study transient stochastic electrochemical events such as collisions of individual nanoparticles and large molecules on an electrode surface. With the help of advanced microscopy tools, such as single-molecule fluorescence and Raman, one can now study the exciting redox behavior of single molecules. Moreover, substantial opportunities have emerged from the use of *in situ* transmission electron microscopy (TEM) to directly observe changes at the electrode/solution interface.

This Review focuses on recent advances in the field of nanoscale electrochemistry since 2013. This topic is "Revisited" because our group authored a review of the field for the 2013 version of this special issue.[1] Therefore, the focus of this Review is on research published since that time. We provide background information citing older literature as needed to give the reader a full view of the topic at hand, but in general, we refer the interested reader to our previous review for a detailed account of the field pre-2013. While we tried to be as comprehensive as possible, as with any review, it is impossible to cover everything. We wish for readers to view this as an account of the most exciting and important recent advances made in the field as seen through our eyes. Along the way, we point out many other reviews dedicated to the specific topics we cover for the interested reader to gain more information and other points of view.

ADVANCED NANOELECTRODES

Naturally, the primary tool for performing nanoscale electrochemistry is a nanoscale electrode, i.e., an electrode with a critical dimension of less than 100 nm. The advantages of shrinking a working electrode down to the nanoscale have been previously discussed.[1−3] These include the ability to do electrochemistry in smaller spaces, at faster time scales, and with higher sensitivity. Harnessing these advantages remains the motivation for continued work in this area. Nanoelectrodes have been used to probe single biological cells,[4] study fast reaction kinetics,[5] measure single nanoparticles,[6] image surfaces with nanoscale spatial resolution,[7] detect single molecules,[8] and investigate fundamental electrochemical phenomena.[9] In other words, nanoelectrodes enable "high-performance" electrochemical measurements to be made that are impossible to carry out using conventional macroscopic electrodes.

To use the electrodes, they must first be made. Nanoelectrode fabrication has not significantly changed since some of the first reports of successful fabrication.[10,11] Basically, a conductive material such as carbon or a noble metal is surrounded by an insulator such as glass or polymer in such a way as to leave a defined area of the conductor exposed. This exposed area then serves as the electroactive area of the electrode. Different fabrication procedures are capable of producing different electrode geometries, including bands, disks, spheres, and hemispheres. The various nanoelectrode fabrication methods have been previously reviewed by our group[1,12] and others,[13,14] and we refer readers to these reviews for more specific details.

Ongoing efforts in nanoscale electrode fabrication are typically focused on adapting established processes to fabricate a desired electrode, usually with a particular end-use in mind. For example, Kim et al. added a step to the well-established laser pulling process to fabricate glass-sealed TiO_2-coated Pt

Special Issue: Fundamental and Applied Reviews in Analytical Chemistry 2016

Published: December 2, 2015

DOI: 10.1021/acs.analchem.5b04542
Anal. Chem. 2016, 88, 414−430

nanoelectrodes for detecting and studying single nanoparticles.[15] These were fabricated by depositing an insulating layer of TiO_2 onto a Pt nanoelectrode. When a nanoparticle contacts the TiO_2 surface, electron tunneling between the particle and Pt can occur, enabling electron transfer between a solution species and the electrode. Liu et al. used a combination of processes to fabricate Au disk nanoelectrodes down to 3 nm in radius, which were then used to monitor dopamine exocytosis from model cells.[16] Their method involved etching an Au microwire to a sharp tip followed by insulation with electrophoretic paint and polyimide. Korchev and co-workers used the pyrolytic deposition of carbon into empty laser-pulled glass capillaries to create a nanoprobe for high-resolution electrochemical imaging, in which one barrel of a pulled dual-barrel capillary was filled with carbon to create a nanoelectrode.[17] This configuration has since been used for mapping pH and topography[18] as well as the electrocatalytic activity of Pt nanospheres.[19] It has also recently been extended to a quad-barrel system[20] that is capable of detecting single redox molecules.[21] Actis et al. used a similar carbon deposition procedure to create single nanoelectrodes with a tunable radius from 5 to 200 nm that were used for single-cell analysis (Figure 1A,B).[22] The researchers functionalized the carbon surface with Pt and were able to insert the electrode into cells to take intracellular electrochemical measurements as well as measurements of brain slices. The Gogotsi and Mirkin groups have also used the pyrolytic deposition of carbon into empty laser-pulled glass capillaries to form nanoelectrodes, which they have used to electrochemically sample atto- to picoliter volumes[23] and to study single nanoparticles.[24]

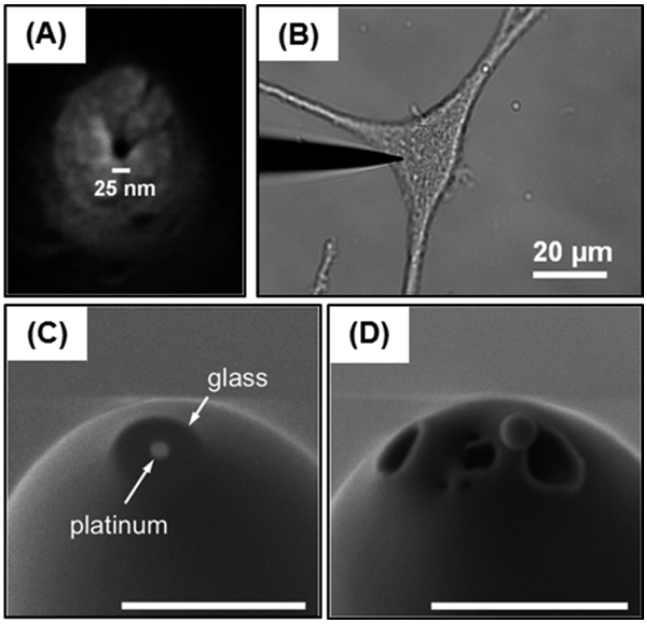

Figure 1. (A) Physical characterization of carbon nanoelectrodes: SEM micrograph of a nanoelectrode tip coated with a thin (~10 nm) layer of Cr. (B) Optical micrograph of a carbon nanoelectrode about to penetrate a melanoma cell for intracellular measurements. (A) and (B) are reproduced from Actis, P.; Tokar, S.; Clausmeyer, J.; Babakinejad, B.; Mikhaleva, S.; Cornut, R.; Takahashi, Y.; Córdoba, A. L.; Novak, P.; Shevchuck, A. I.; Dougan, J. A.; Kazarian, S. G.; Gorelkin, P. V.; Erofeev, A. S.; Yaminsky, I. V.; Unwin, P. R.; Schuhmann, W.; Klenerman, D.; Rusakov, D. A.; Sviderskaya, E. V.; Korchev, Y. E. *ACS Nano* **2014**, *8*, 875−884 (ref 22). Copyright 2014 American Chemical Society. (C) and (D) SEM images of an ~110 nm-diameter Pt nanoelectrode (C) before and (D) after electrostatic discharge damage. Reproduced from Nioradze, N.; Chen, R.; Kim, J.; Shen, M.; Santhosh, P.; Amemiya, S. *Anal. Chem.* **2013**, *85*, 6198−6202 (ref 25). Copyright 2013 American Chemical Society.

As can be expected, nanoelectrode fabrication is a time-consuming and difficult process. The behavior of nanoscale electrodes crucially depends on the fabrication method employed and the manner with which they are handled during fabrication and use. As an example of the latter, Amemiya and co-workers have shown that even small amounts of static discharge can destroy nanoscale electrode surfaces or cause their electrochemical etching (Figure 1C,D).[25] The thickness and morphology of the surrounding insulator can also have a dramatic impact on the behavior of a nanoelectrode. Limiting current measurements, which are often used to estimate electrode size, are only accurate if the geometry of both the electrode and the surrounding insulator are known.[26] A recent study by Compton and co-workers shows that the thickness of the surrounding insulator can have a large effect on the diffusion-limited steady-state current.[27] As is evident, full characterization of a nanoelectrode typically requires some type of imaging in addition to electrochemical measurements. Typical imaging methods include electron microscopy, atomic force microscopy (AFM), and scanning electrochemical microscopy (SECM). As it is nearly impossible to produce two identical nanoelectrodes using current fabrication techniques, each electrode must be separately characterized, making this a tedious task.

Care must also be taken, especially when using polymers for insulation, to avoid flaws such as pinholes or cracks which can expose underlying electrode surfaces to the working solution and thus significantly and unknowingly increase the electrode's electroactive area. Optical imaging techniques, such as electrochemical precipitation of fluorophores at active sites followed by fluorescent imaging, can be useful in identifying these defects.[28] Additionally, one must ensure that the electrode surface is free from contaminants, as they can also distort the electrode's response. While polishing can be used for larger electrodes, nanoelectrodes are more delicate and polishing can significantly change the size and morphology of the electrode and surrounding insulator. To address this, Mirkin and co-workers recently introduced a plasma cleaning procedure.[29]

Even with great care, ideal materials, and refined procedures, reproducibly fabricating nanoelectrodes with well-defined geometries at high yield remains a big challenge. A method able to do this would be of immense value to the field, saving researchers significant time and resources that are otherwise dedicated to the tedious low-yield fabrication and individual characterization of nanoelectrodes required by current methods. We venture the prediction that modern lithography and microfabrication techniques may be used to solve this problem by batch-producing quantities of identical electrodes. However, as of now, the solution to this challenge remains to be seen. Nanoelectrodes as a tool of central importance have provided enormous potentials in the area of nanoscale electrochemistry. Previous research has been heavily focused on several key areas including high-resolution electrochemical imaging with SECM, study of cellular activity such as exocytosis, single nanoparticles and single molecules, and fundamental studies of redox processes and double layer effects. New and exciting applications of nanoelectrodes will likely

DOI: 10.1021/acs.analchem.5b04542
Anal. Chem. 2016, 88, 414−430

emerge in the near future. Some exciting examples may include the combined use of nanoelectrode probes with various spectroscopies and the use of nanoelectrodes to study nucleation of solid particles and gas nanobubbles.

NANOPORE ELECTROCHEMISTRY

Over the past couple of decades, research in the utilization of nanopores as a unique electroanalytical sensing tool has experienced intensive growth. While nanopore detection had humble beginnings in the 1950s with the Coulter counter, which required the user to count translocating blood cells through a pinhole,[30] development and use of micro- and nanofabrication tools and techniques have led to substantial advancements and encouraged additional research efforts. The modern nanopore sensor operates by resistive-pulse detection and consists of a biological or solid-state membrane containing a 1−500 nm diameter pore and electrolyte solution on each side. A potential is held across the membrane, and the transmembrane ionic current is monitored as a function of time. Translocation of an analyte object (e.g., a molecule, nanoparticle, or cell) through the pore due to an electrophoretic driving force or pressure-driven flow causes the resistance of the system to change, which is detected by a change in ionic current (Figure 2).[31] The amplitude of the

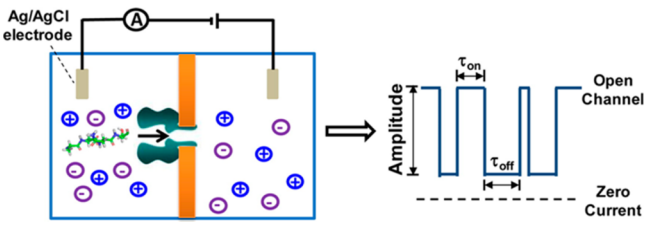

Figure 2. Schematic representation of nanopore resistive-pulse detection using a protein pore. Reproduced from Wang, G.; Wang, L.; Han, Y.; Zhou, S.; Guan, X. *Acc. Chem. Res.* **2013**, *46*, 2867−2877 (ref 31). Copyright 2013 American Chemical Society.

measured current pulse is proportional to the object's size, while the duration of the pulse can yield information about the object's translocation time, behavior in the pore, and surface charge.[1,32−34] Nanopore detection has proven amenable to a wide range of analytes, including single-stranded DNA (ssDNA) for base sequencing,[35] RNA,[36] biomarker-modified DNA,[37−39] proteins,[40] viruses,[41,42] small molecules,[43,44] and nanoparticles.[45] Nanopore-based DNA sequencing methods have received considerable attention in recent years, and we refer the interested reader to other reviews for more detailed information on the topic.[46,47] Significant advantages of nanopore sensors include high sensitivity with single-molecule detection capabilities[31] and an increasingly low cost to implement,[48] while perhaps the largest limitation has been the difficult fabrication processes required to produce pores with controlled dimensions. We will highlight some of the significant advances in fabrication and detection capability that have been made in both biological and solid-state types of devices within recent years. For further information, we refer the interested reader to a recent review dedicated to the topic.[49]

Solid-state nanopores are typically fabricated from materials such as silicon nitride or silicon dioxide, and their fabrication has historically been time-consuming, expensive, and difficult to reproduce. Such fabrication methods include ion-beam drilling[50] and electron-beam structuring by use of a TEM.[51,52] An exciting new fabrication technique termed controlled dielectric breakdown (CDB) has been demonstrated by Tabard-Cossa and co-workers. CDB produces near-perfect yields, is comparably cheap, and can be automated in the creation of individual nanopores down to 2 nm in diameter with subnanometer precision.[48,53] The method works by applying a constant potential across a thin dielectric membrane while measuring the leakage current. A sudden increase in leakage current indicates that a pore has been formed, and its size can be precisely tuned by applying short alternating voltage pulses.[48] The size of a cylindrical pore can be determined by either correlating the measured conductance to pore diameter using a known equation[54] or imaging with electron microscopy. CDB has been shown to be effective for thin silicon nitride membranes, while a similar electrical pulse fabrication technique has been demonstrated as a viable method for graphene nanopore fabrication.[55] Pores fabricated via CDB have been used to detect ssDNA[56] and have been successfully integrated within microfluidic channel arrays.[57] Although the practical procedure is simple and the mechanism of formation has been extensively studied,[58] a major limitation to CDB is the unpredictable position of pore formation. Typical experiments utilize a 5 μm × 5 μm silicon window to localize the formation. Due to the difficulty of finding 2 nm pores within that space, a new modification to CDB has been created. Microfabricated gold structures are used to localize a high voltage field to a precise location via plasmonic excitation, thereby directing the location of the nanopore to a predictable postion.[59] The quality of these pores is comparable to TEM drilling, making CDB a high-yield, low-cost alternative for solid-state nanopore fabrication.

Biological nanopores have also been heavily utilized in resistive-pulse detection, most prominently for ssDNA sequencing, although additional detection applications have been demonstrated as well. These nanopores have generally been created by use of proteins that insert themselves into a lipid bilayer and assemble into transmembrane channels.[60,61] Two commonly used biological pores are α-hemolysin (α-HL), extracted from the bacteria *Staphylococcus aureus*,[62] and *Mycobacterium smegmatis* porin A (MspA). Both α-HL and MspA contain a constricted inner-pore diameter of about 1 nm, but they vary in pore length.[63] The use of these pores has shown success in ssDNA sequencing, most notably with the ability to distinguish the four canonical DNA bases using MspA by immobilizing the polynucleotide inside the pore.[64] Recent work utilizing α-HL nanopores involves the detection of aromatic,[38] thiol-substituted,[37] and other biomarkers on DNA,[39] RNA polynucleotide sequences,[65,66] and synthetic polymer chains.[67] Despite the noteworthy successes for nanopores formed by α-HL and MspA, limitations arise in the detection of molecules structurally larger than the approximate 1 nm inner-pore diameter and in environments where lipid bilayers are unstable.[68]

An alternative approach for biological nanopore fabrication that enables structural customization is a technique called DNA origami. Unlike protein-based nanopore structures, this bottom-up self-assembled scaffolding approach uses a single long ssDNA chain along with multiple shorter ssDNA chains as binders to systematically create predetermined shapes, demonstrated in Figure 3 in the shape of a nanopore framework.[69,70] This approach was first demonstrated in 2006,[69] and further development has been aided by the design of CAD software that enables precise structural fabrication.[71,72]

DOI: 10.1021/acs.analchem.5b04542
Anal. Chem. 2016, 88, 414−430

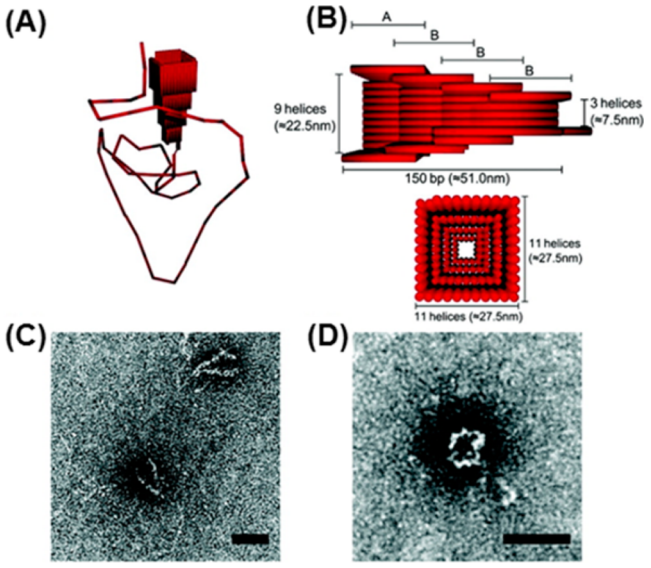

Figure 3. (A) Schematic representation of DNA origami nanopore structure, where the double helices are presented as rods. (B) Top: Side view of DNA origami nanopore structure, where the overall length of the nanopore is 150 bp (51.0 nm) with the smallest opening of 7.5 × 7.5 nm^2. Bottom: Top-view of the structure showing that the square shape is 11 by 11 helices with a total area of 27.5 × 27.5 nm^2. (C) TEM images of assembled DNA origami nanopores negatively stained with uranyl acetate. (D) TEM image of upright standing DNA origami nanopore. Scale bars = 40 nm. Reproduced from Bell, N. A. W.; Engst, C. R.; Ablay, M.; Divitini, G.; Ducati, C.; Liedl, T.; Keyser, U. F. *Nano Lett.* **2012**, *12*, 512−517 (ref 74). Copyright 2012 American Chemical Society.

In addition to specific structure manipulation, DNA origami nanopores enable cavity modification via selected use of specific nucleic acid sequences. Recent studies have modified existing glass nanocapillary supports with an origami nanopore to study its voltage-dependent properties[73] and DNA translocation capabilities,[74] showing that resistive-pulse detection is possible using this approach.

In addition to the array of materials and methodologies developed for nanopore detection, recent studies have demonstrated unique solutions for persistent challenges. With the use of pure electrical measurements for resistive-pulse detection, two common limitations arise, namely, control of translocation speeds and electrical noise.[75] Rapid translocation speeds can produce poor resolution of individual ionic current pulses, making each detection event difficult to distinguish. Perhaps the most promising modification to nanopore sensing that addresses these problems is the combination of electrical measurement with established optical techniques, as described in an excellent review by Gilboa and Meller.[75] They evaluated the implementation of techniques such as total internal reflectance fluorescence microscopy and confocal microscopy, along with various background suppression methods, and show that their use can produce promising results in mitigating background noise and in controlling translocation speeds of DNA and proteins. In addition to the new nanopore fabrication methods and demonstrated applications previously mentioned, these optical technique results show promise of powerful new detection capabilities for nanopores, encouraging the continued study and further development of this electroanalytical technique.

NANOPARTICLE ELECTROCHEMISTRY

Metal nanoparticles (NPs) have found a wide range of applications due to their large surface-to-volume ratio, size and shape-dependent electronic and optical properties, and high density of active sites. The electrocatalytic properties of NPs are of particular interest to scientists because NPs are involved in numerous electrocatalytic processes that are important for energy production, environmental protection, synthesis, etc. The electrochemical activities of NPs are mainly determined by NP material, size, shape, and surface structure. Obtaining a better understanding of the structure−function relationship of NPs is fundamental for designing better electrocatalysts. Assessing the activity of individual NPs is desired due to the intrinsic heterogeneity among these NPs. The ability to study single NPs enables the study of how each physical parameter affects NP catalytic activity. Extensive efforts have been devoted to developing electrochemical methods to study single NPs. Here, we review the recent important advances in single-nanoparticle electrochemistry. There are also some existing reviews about single-NP catalysis and electrocatalysis that cover longer time periods for readers who are interested in earlier developments and more details related to this topic.[76−78]

Nanoparticle Collisions. Electrochemical detection of single nanoparticles via stochastic particle collision with an electrode has become a particularly useful method because it is simple and fast and enables detection in solution. As such, it has received considerable attention in recent years. Xiao and Bard first developed this method of electrocatalytic current amplification via stochastic single-nanoparticle collisions.[79] In this method, a detection UME is immersed in a solution containing an electroactive species and dispersed NPs. The detection UME is held at a potential where the faradaic reaction of the electroactive species does not occur on its surface but can be catalyzed on the NPs when they randomly collide and stick to the UME. Therefore, each NP collision event results in a discrete current step. Information about the catalytic NPs such as size distribution, concentration, and diffusion coefficient can then be obtained from these current transients. This method has been extended to various experimental systems, with several developments in this important field emerging since our previous review.[1]

One important development is that the technique has been applied to studying NPs of broader types of materials, going beyond noble metal nanoparticles. For example, Compton and co-workers successfully detected and sized fullerene NPs in a nonaqueous solution.[80] Additionally, Pumera and co-workers studied the NP collision of four transition metal dichalcogenides in both the cathodic and anodic regions.[81] Other types of NPs such as TiO_2,[82] CeO_2,[83] ZnO,[84] and Mo[85] have also been detected and studied by this method. Besides the "hard particles" such as metal and metal oxide NPs, it has been shown that it is also possible to detect "soft particles" such as emulsion droplets via single NP collision. Bard and co-workers have reported two methods for soft particles: the "emulsion droplet reactor (EDR)" method and the "emulsion droplet blocking (EDB)" method (Figure 4A).[86−88] In the EDR method, an electroactive species is added to the emulsion droplet. A current spike is observed when the emulsion droplet collides with the detection electrode and the electroactive species is oxidized or reduced. If the droplet contains a luminophore and a coreactant, electrogenerated chemiluminescence (ECL) re-

DOI: 10.1021/acs.analchem.5b04542
Anal. Chem. 2016, 88, 414−430

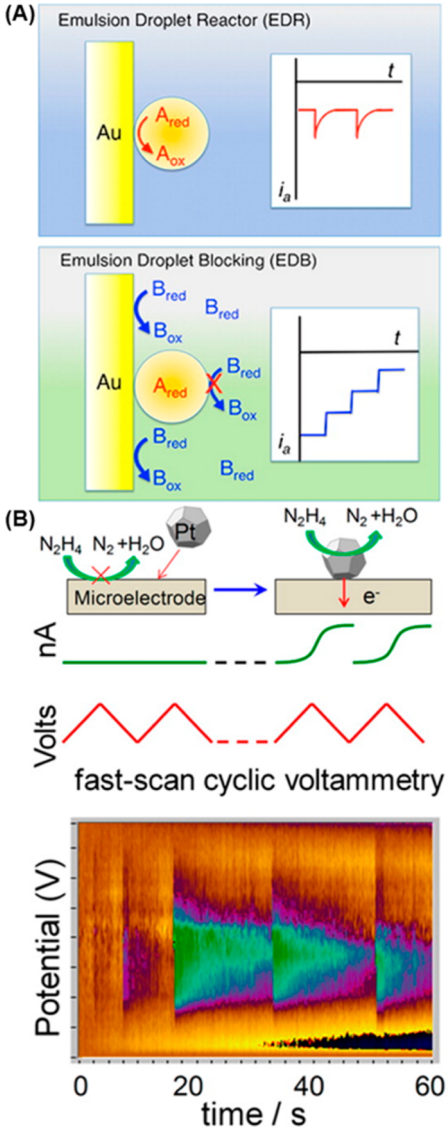

Figure 4. Single nanoparticle collision-based electrochemistry. (A) Schematic diagram of two suggested emulsion collision methods. Reproduced from Kim, B. K.; Boika, A.; Kim, J.; Dick, J. E.; Bard, A. J. *J. Am. Chem. Soc.* **2014**, *136*, 4849−4852 (ref 87). Copyright 2014 American Chemical Society. (B) FSCV detection of single-particle collisions: (top) diagram of a single NP collision at a UME monitored by FSCV. A triangular voltage waveform is continuously scanned on the probe UME and the background-subtracted faradaic response is monitored. (bottom) A characteristic 60 s FSCV trace; the color plot represents 6000 continuously recorded, background-subtracted CVs. Reproduced from Guo, Z.; Percival, S. J.; Zhang, B. *J. Am. Chem. Soc.* **2014**, *136*, 8879−8882 (ref 103). Copyright 2014 American Chemical Society.

sponses can also be simultaneously monitored.[89] In the EDB method, a high concentration of a redox active species was added to the continuous phase. The detection of the emulsion droplet is shown as a current decrease due to a partial blockage of the active electrode surface by the droplet particle. The detection of other types of "soft particles" such as liposomes, vesicles, and micelles through single-particle collision has also been reported.[90−94]

Another advancement in single NP collision electrochemistry is the fabrication and use of new types of detection electrodes. Wakerley et al. reported the fabrication and use of boron-doped diamond (BDD) disk UMEs for investigating hydrazine oxidation at single Au and Pt NPs.[95] The BDD electrodes are good for NP collision experiments because they are electrocatalytically inactive and have low background currents. Stevenson and co-workers have demonstrated the use of a renewable Hg-modified Pt UME (Hg/Pt UME) for NP detection.[96] The uniqueness of this detection electrode is that it poisons the catalytic NP once it contacts the Hg/Pt UME surface and deactivates the catalytic reaction. As a result, the current increase caused by the reaction decays to the background current level, displaying a spike-like current response. An increased signal-to-noise ratio was also achieved because of the suppressed background current. Besides monitoring the amperometric response, they have also reported a potentiometric method for detecting single Pt NPs using the Hg/Pt UME with high sensitivity.[97] Bard and co-workers have used electrodeposition of a thin amorphous TiO_2 layer to passivate an electrode surface to minimize the background current.[15,98] However, the TiO_2 film is thin enough to allow electron tunneling to a metal NP that is in contact with it. Therefore, when a metal NP collides on the ultrathin TiO_2 layer, the faradaic reaction of redox species in solution is turned on and a collision signal is observed.

The particle−electrode collision method can be further improved by combining electrical detection with optical detection, such as fluorescence or ECL. By incorporating fluorescence microscopy, Crooks and co-workers simultaneously detected electrochemical and optical signals of single fluorescent microbeads colliding on a UME and have shown that these two kinds of signals can be directly correlated.[99] The optical tracking provided additional information from individual particles, such as the relationship between the collision location and the magnitude of current steps. Bard and co-workers have coupled electrical and ECL detection together for monitoring the collision of single attoliter oil droplets.[89] In this work, rubrene and tri-*n*-propylamine (TPrA) were added to the oil droplets to serve as an ECL luminophore and a coreactant, respectively. During the collision, a current blip was observed when the constituents within the droplet were oxidized, and an ECL blip was also detected from the follow-up reactions. The current and ECL responses were correlated to calculate the droplet size and its content. However, as a photomultiplier tube was used as the detector, no spatial information on the collision events was gained. Besides optical tracking, external magnetic fields have also been incorporated in some systems to control particle−electrode collisions and to improve the collision frequency.[100−102]

Previously, a limitation in the NP collision technique was the lack of chemical information, as conventional amperometry only provides information about transient current−time responses at a constant potential and is unable to identify the catalytic NP material. To overcome this, our group recently employed fast-scan cyclic voltammetry (FSCV) to study single NP collisions (Figure 4B).[103] In this study, a fast and repetitive voltage signal (typically 50−500 V/s) was continuously scanned on the detection UME, and its current response was recorded. The transient voltammetric response of single catalytic NPs as they collided and stuck to the detection electrode could thus be obtained. NPs of Pt and Au could be further identified from a mixed solution of these two types of NPs by examining each voltammogram extracted. Therefore, compared to previous amperometric methods, the use of FSCV enabled us to acquire important chemically resolved

DOI: 10.1021/acs.analchem.5b04542
Anal. Chem. 2016, 88, 414−430

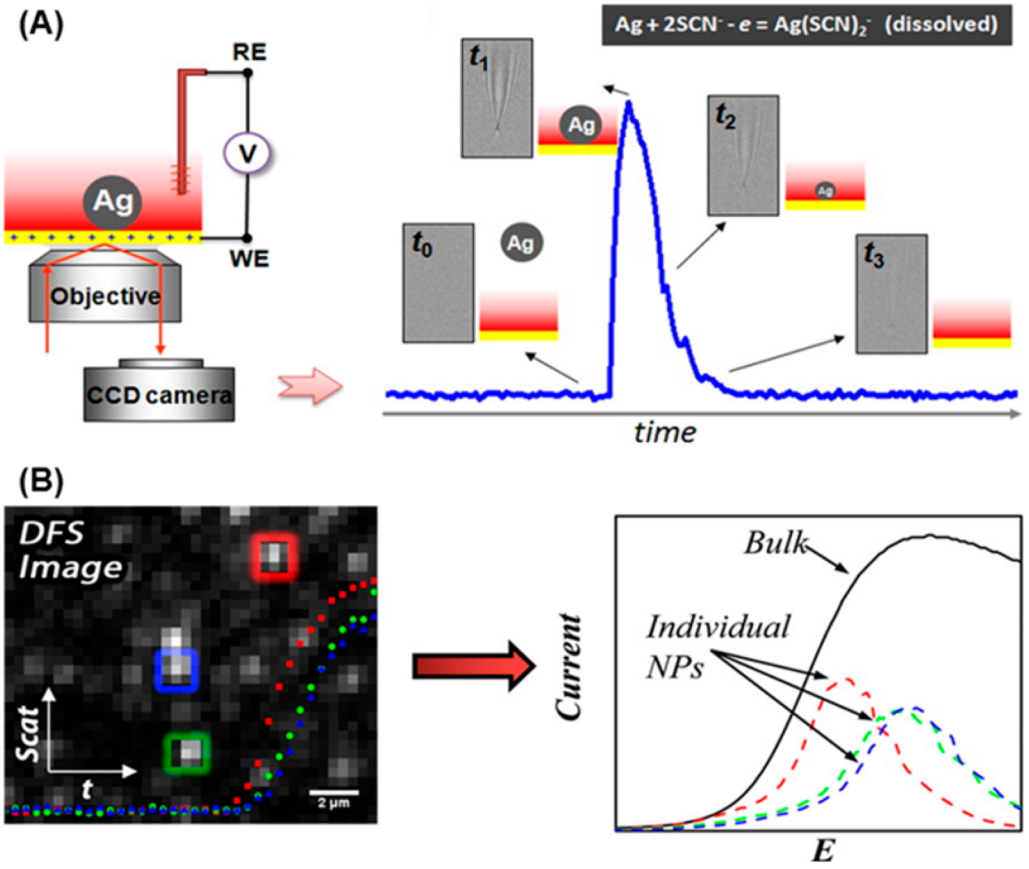

Figure 5. Plasmonic approaches for single nanoparticle electrochemistry. (A) Plasmonic imaging of single Ag NPs. (left) Schematic illustration of P-ECM imaging of single NP electrochemistry. (right) Transient collision and electrochemical oxidation of a single Ag NP correlated with the transient plasmonic image intensity (blue curve). Reproduced from Fang, Y.; Wang, W.; Wo, X.; Luo, Y.; Yin, S.; Wang, Y.; Shan, X.; Tao, N. *J. Am. Chem. Soc.* **2014**, *136*, 12584−12587 (ref 109). Copyright 2014 American Chemical Society. (B) Dark-field scattering spectroelectrochemistry used to analyze the electrochemical formation of individual Ag NPs. Single NP light scattering intensity (left) is related to particle size, enabling rapid particle size determination and the construction of voltammetric curves for individual NPs (right). Reproduced from Hill, C. M.; Pan, S. *J. Am. Chem. Soc.* **2013**, *135*, 17250−17253 (ref 110). Copyright 2013 American Chemical Society.

information in addition to the transient current response for single NPs.

Single-Nanoparticle Immobilization. Single-particle immobilization on a nanoelectrode continues to be a key method to isolate a single NP for electrochemical characterization. Our group has studied the electrocatalytic activity of a single Au NP by chemically immobilizing an Au NP onto a chemically modified Pt nanodisk electrode.[104] Sun and co-workers have investigated the electrochemical stability of single Au NPs protected by a single monolayer by directly adsorbing an Au NP onto a nanometer-sized Pt electrode.[105] They have found that, as the radius of the particle becomes smaller, it is more difficult to oxidize the Au NP or reduce its oxide. More recently, Sun et al. reported the study of the electrochemical behavior of a single "naked" Au NP that was spontaneously formed on the surface of a Pt nanoelectrode under open circuit potential.[106] The electrochemical results showed that the Au NP displayed extraordinary stability compared to its bulk phase.

Mirkin and co-workers reported using nanometer-size carbon electrodes as substrates for the immobilization of single Au NPs.[24] The Au NPs were attached to the carbon nanoelectrodes through three methods: direct adsorption onto the carbon surface, electrostatic attachment to a polyphenylene film, or covalent linkage via the reduction of an aryl diazonium salt. The activity toward the hydrogen evolution reaction (HER) of single Au NPs was studied, and it was found that the activity toward the HER of an Au NP electrostatically attached to the polyphenylene film was lower than an Au NP adsorbed directly onto the carbon nanoelectrode surface.

Bard and co-workers developed a method of fabricating nanometer-size electrodes based on a metal/insulator/NP system.[15] An insulating TiO_2 film was deposited onto a Pt UME surface to block electron transfer to a solution species, followed by attachment of a single metal NP to the insulating film via random NP collision. The electron transfer to the solution species could be restored when the metal NP was in contact with the insulating film. When the entire electrode was removed from the NP solution and immersed into a new solution containing electroactive species, typical UME CVs could be recorded and the electrochemical behavior of the single metal NP could be investigated.

Plasmonic Approaches for Single Nanoparticles. Plasmonic-based electrochemical current microscopy (P-ECM) is a nice technique initially developed by Tao and co-workers for imaging electrochemical reactions of NPs.[107,108] Recently, the group used this technique to detect the transient electrochemical oxidation of single Ag NPs during collision with a detection electrode and studied the oxidation kinetics of the reaction by performing voltammetry (Figure 5A).[109] Since the plasmonic image intensity decreases as the Ag NPs decrease

DOI: 10.1021/acs.analchem.5b04542
Anal. Chem. 2016, 88, 414−430

in size during oxidation and the change in the NP volume is proportional to the amount of charge transferred during oxidation, the local electrochemical current of individual NPs could be determined and the size-dependent electrochemical activities of single Ag NPs could be investigated.

Dark-field microscopy is often utilized to measure the localized surface plasmon resonance (LSPR) spectrum of a single plasmonic NP. Hill and Pan used dark-field scattering microscopy to track the electrochemical formation of individual Ag NPs at the surface of an indium tin oxide (ITO) electrode (Figure 5B).[110] In their system, when the potential at the ITO electrode is swept cathodically, Ag NPs start to grow on the electrode through the reduction of Ag^+ ions in solution. The formation of these Ag NPs can be imaged from light scattering. The actual size of the deposited Ag NPs was measured by scanning electron microscopy (SEM) and correlated to the light scattering intensity. With the NP scattering−size correlation and the scattering−potential relation, it was then possible to calculate the Faradaic current for Ag^+ reduction contributing to the formation of a given Ag NP. In this way, voltammetric curves for individual NPs could be constructed on the basis of the scattering intensities at different applied potentials. More recently, Pan's group has further studied the subsequent oxidation of Ag NPs on the ITO electrode using this method.[111] Dark-field microscopy has also been employed to study electrochemical heterogeneity of single Au NPs.[112,113] While the plasmonic approach to single-nanoparticle catalysis is promising, it still has the limitation of requiring a plasmonic material of sufficient size in order to be observed.

Scanning Electrochemical Cell Microscopy for Single Nanoparticles. Developed by Unwin and co-workers, this technique employs scanning electrochemical cell microscopy (SECCM)[114] to detect and characterize individual electrocatalytic NPs.[115] In this approach, a theta pipet is filled with an electrolyte solution with dispersed NPs and two quasi-reference counter electrodes. A micro- or nanoscopic electrochemical cell is then constructed when a liquid meniscus is formed between the pipet tip and the substrate. The wetted area of the substrate acts as the working electrode, and current steps can be observed as a single NP lands onto the substrate and catalyzes a redox reaction in a manner similar to that in a traditional NP collision experiment. Since the pipet tip is small (~1.5 μm in diameter), the resulting meniscus area and, hence, the working electrode area are also small. The background current is thus very low, enabling the detection of very small current signals. One major advantage of this technique over the traditional single NP collision experiment is that it enables a much broader range of substrates to be studied, negating the need for fabricating detection electrodes with complex structures. In this report,[115] the landing of Au NPs on highly oriented pyrolytic graphite (HOPG) and on a carbon-coated TEM grid was observed and the potential-dependent activity of Au NPs was studied. TEM was used to characterize the NPs after they landed onto a TEM grid. Also, a cyclic voltammogram of the first single Au NP landed was recorded by sweeping the substrate potential. In this way, the electrochemical and physical characterization of a single Au NP could be performed.

In a more recent report, Unwin and co-workers further analyzed the current−time transients of ruthenium oxide NPs landing on an HOPG substrate using H_2O_2 oxidation as an indicator reaction.[116] They observed NP impacts with very high frequency and proposed repetitive trapping and release of an individual NP as the cause. In another report, they used SECCM to detect single Au NP collisions on alkanethiol-modified Au electrodes with different terminal groups such as −COOH, −OH, and $-CH_3$.[117] They found that the collision signals had different characteristics, indicating that the NP−electrode interactions were greatly influenced by the different terminal groups. AFM was further used to probe the interactions via measuring interacting forces between citrate-modified Au-coated AFM tips and the alkanethiol-modified Au substrates. These studies show that SECCM has become a very useful method for studying the interaction between a NP and an electrode surface during NP collision.

SECM is another technique that has recently been utilized for studying single catalytic NPs. However, we include those studies as part of the section in this Review specifically covering recent developments in SECM.

SINGLE-MOLECULE ELECTROCHEMISTRY

The main motivation for single-molecule detection is straightforward: it represents the fundamental lower limit of detection for an analytical technique. With single-molecule detection, one can begin to probe molecular heterogeneities, build single-molecule sensors, and understand chemical and biological processes on a single-molecule level. It can also be a gateway to new techniques, as demonstrated with single-molecule detection via fluorescence being developed into super-resolution localization microscopy.[118] While single-molecule detection has become routine in other analytical techniques, electrochemical detection of single molecules has proven to be more difficult. This Review will focus on work describing single-molecule detection via faradaic response, leaving out the interesting area of single-molecule junctions, which has been recently reviewed elsewhere.[119,120] We focus on two main methods of signal transduction: direct electrical detection and optical detection. Each method has its advantages and disadvantages. Electrical detection enables a direct signal transduction pathway and is readily amenable to parallelization via microfabrication techniques, yet is not capable of detecting single faradaic reactions and therefore requires averaging over many redox events to produce a detectable signal. On the other hand, optical detection is capable of detecting single redox events and can provide spatially resolved images of those events, yet only certain redox molecules have the requisite optical properties for detection. Significant progress has been made in both areas over the past few years as work has begun to move beyond the proof-of-concept phase.

Direct Electrical Detection. The direct electrical detection of single electrochemically active molecules is experimentally difficult due to the small faradaic charge passed by a single molecule. For a typical faradaic reaction, only a few electrons are transferred per molecule, which has made electrical detection of single electron transfer reactions impossible thus far. In order to detect the faradaic signal from a single molecule, some type of signal amplification is needed in which the number of electrons passed per unit time (i.e., the current) is increased. As we have noted in our previous review[1] and others have noted in more recent reviews,[122,123] the method successfully used to achieve this signal amplification has been redox cycling of trapped molecules in thin-layer electrochemical cells. In this configuration, two parallel electrodes are placed close together and biased such that a randomly diffusing analyte molecule trapped between them will be oxidized at one electrode and reduced at the other. Thus, the analyte molecule effectively becomes a shuttle carrying electrons between the

DOI: 10.1021/acs.analchem.5b04542
Anal. Chem. 2016, 88, 414−430

two electrodes, transferring n (n is typically only one or two) electrons per round trip. In practical terms, to provide sufficient current amplification, the two electrodes must be placed within ~100 nm or less.[121] For an ideal situation in which Brownian motion is the only transport consideration and the reaction kinetics are not limiting, the steady-state current of a single trapped analyte molecule, i, can be given by $i = (enD)/L^2$, where e is the elementary charge, n is the number of electrons transferred per reaction, D is the diffusion coefficient of the analyte, and L is the distance between the two electrodes.[8] As is clearly seen, electrode spacing is a crucial determinant of the current, with smaller distances giving increased amplification.

Fan and Bard were the first to use redox cycling of trapped molecules in a thin-layer cell to electrochemically detect single molecules.[8,124,125] In their pioneering experiment, they trapped single molecules in a ~10 nm gap between a slightly recessed wax-insulted SECM tip nanoelectrode and a substrate electrode.[8] Their configuration enabled a current of ~1 pA to be generated from single (ferrocenymethyl)-trimethylammonium ($FcTMA^+$) molecules, meaning an analyte molecule could make ~10^7 round trips between the electrodes per second. More than a decade later, Sun and Mirkin used a similar scheme to achieve single-molecule electrochemical detection by using a slightly recessed platinum nanopore electrode in contact with a Hg pool electrode.[126] Single redox molecules could be trapped in the nanopore and then cycled between the Pt and Hg electrodes.

More recently, the Lemay group has produced a body of work on electrochemically detecting single molecules, albeit using a slightly different approach that is focused on using cells microfabricated with standard lithography techniques (Figure 6A). These have several advantages over the tip-based cells of Bard and Mirkin, including higher reproducibility, parallel fabrication capabilities, easier characterization of cell geometry, and the ability to easily add design complexity (i.e., alteration of geometry, integration with microfluidics, formation of arrays) for future applications.[121] Their group first reported a device capable of single-molecule detection in 2011.[127] In that report, two Pt electrodes were fabricated with an interelectrode spacing of 70 nm, and single molecules of ferrocene in acetonitrile were detected via redox cycling, with one ferrocene molecule producing ~20 fA of current. Importantly, the current from each electrode could be monitored separately, resulting in current signals that were anticorrelated when detection occurred.

Lemay's group then improved the device by lessening the dead volume in the cell and shrinking the electrode spacing to 40 nm, resulting in greater current amplification (Figure 6B,C).[128] This device was used to detect single redox molecules in aqueous solutions, something not possible in their previous device due to the diffusion coefficient of redox molecules in water being lower than in normal organic solvents. This report represents a significant step forward in developing single-molecule electrochemical detection into useful (bio)assays. Toward that end, Lemay's group has recently integrated enzyme detection into their thin-layer devices.[129] They report being able to detect ~5000 tyrosinase enzymes that are immobilized in their device by measuring the redox-active product created by the enzymatic conversion of an inactive substrate. Importantly, their method enabled the real-time monitoring of enzymatic activity from a conversion that has a turnover rate of only 14 molecules per second per enzyme, boding well for the possibility of measuring single-enzyme kinetics with this method in the future. Lemay's reports also note that the current measured from single molecules is significantly lower than that predicted by the diffusion-limited steady-state equation and provide evidence that reversible adsorption of molecules onto the electrodes significantly contributes to this.[127,128] Further experimental work by Lemay[130] and theoretical work by Wolfrum[131] have supported this idea and led to some very interesting insights about redox molecule adsorption onto electrodes.

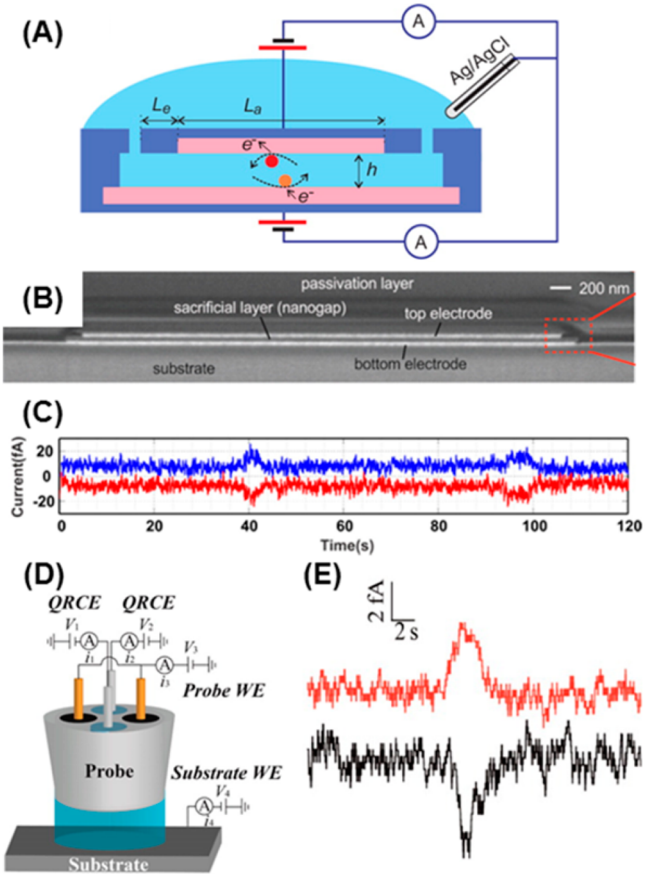

Figure 6. Electrical single-molecule detection via redox cycling. (A) Schematic diagram of a cross-section of Lemay's nanogap thin-layer cell used for single-molecule detection. The two electrodes are shown in pink. Reproduced from Mampallil, D.; Mathwig, K.; Kang, S.; Lemay, S. G. *J. Phys. Chem. Lett.* **2014**, *5*, 636−640 (ref 130). Copyright 2014 American Chemical Society. (B) SEM image of a cross-section of a nanogap thin-layer cell with an interelectrode spacing of 40 nm. (C) Single-molecule detection of $FcTMA^+$ in a nanogap device: Current−time traces simultaneously obtained at the top (blue) and bottom (red) electrodes under redox cycling conditions. Discrete, anticorrelated current steps with amplitude ~7 fA are generated each time that an individual $FcTMA^+$ molecule enters and subsequently exits the nanogap. Reproduced from Kang, S.; Nieuwenhuis, A. F.; Mathwig, K.; Mampallil, D.; Lemay, S. G. *ACS Nano* **2013**, *7*, 10931−10937 (ref 128). Copyright 2013 American Chemical Society. (D) Schematic of the electrode configuration for Unwin's quad-barrel device: the carbon working electrodes in the barrel of the probe; two open barrels filled with electrolyte and AgCl-coated Ag wire QRCEs; and the substrate working electrode. (E) Single-molecule detection in the quad-barrel device: Current−time plot for a solution containing 100 nM $FcTMA^+$ in ionic liquid. Reproduced from Byers, J. C.; Nadappuram, B. P.; Perry, D.; McKelvey, K.; Colburn, A. W.; Unwin, P. R. *Anal. Chem.* **2015**, *87*, 10450−10456 (ref 21). Copyright 2015 American Chemical Society.

DOI: 10.1021/acs.analchem.5b04542
Anal. Chem. 2016, 88, 414−430

There have been two very recent reports on electrochemical single-molecule detection. The first is an interesting theoretical piece by Feldberg and Edwards[132] in which the authors develop a model to describe a trapped, single redox molecule in a closed thin-layer cell. This model is meant to represent an idealized version of the previously described single-molecule redox cycling experiments. This model leads to the interesting conclusion that electron shuttling across the electrodes via the redox molecule is the result of two discrete steps: reduction of the redox molecule at one electrode followed by oxidation of the redox molecule at the other electrode, with the faradaic process at an electrode being coupled to a purely capacitive process at the opposite electrode. Therefore, if instrumentation was capable of measuring this, one electron shuttled across the electrodes would result in two discrete current blips, each having a charge of less than *ne*. Importantly, the model also leads to the single-molecule steady-state current formula.

The other recent report belongs to the Unwin group, who presented an interesting new experimental strategy for single-molecule detection via redox cycling (Figure 6D,E).[21] The authors use a pulled, four-barrel glass pipet (~3 μm tip diameter) to create a thin-layer cell. Two of the barrels were filled with carbon and served as the working electrode, while the other two barrels were filled with redox solution and reference electrodes. The redox solution formed a meniscus that covered the carbon working electrodes; this meniscus was then brought into contact with a substrate working electrode, thereby creating a thin-layer cell in which redox molecules could cycle between the carbon working electrodes and substrate working electrode. This creative experimental design, in which the redox solution is confined to a very small droplet and the carbon working electrodes have a very small surface area, enables the current to be measured from both the carbon and substrate electrodes with noise levels of only a few fA. The advantage of such a low noise level was elegantly demonstrated via the detection of single redox molecules in ionic liquid (a relatively viscous media), which resulted in peak currents of only ~4 fA. Additional benefits of this experimental scheme, including the ability to easily substitute the substrate electrode and the ability to precisely change and measure the gap size, make this an exciting development in single-molecule electrochemical detection.

Recently, the Bard group has extended their collision detection experiments down to the single macromolecule regime.[133] This represents a unique detection scheme as compared to other single-molecule electrochemical detection methods. The group oxidized a high concentration of ferrocyanide on a submicrometer radius Pt electrode to generate a steady background current. When electrochemically inactive entities adsorbed onto the electrode surface, part of the diffusive flux of ferrocyanide to the electrode surface was blocked, thus leading to a decrease in current and a transient $i-t$ response. The group was able to detect single proteins and DNA macromolecules using this method. This technique greatly differs from other electrochemical single-molecule detection techniques, especially in that it is used to detect redox inactive molecules. The method's simplicity makes it attractive, and it may prove useful in studying adsorption events at the single-molecule level. It will be very interesting to see how small of an adsorption "foot print" can be detected by this method.

Optical Detection via Fluorescence. The approach of optically detecting single redox molecules has received much attention in recent years. This is in large part due to the successful development of optical techniques for single-molecule detection, such as fluorescence microscopy and surface-enhanced Raman scattering (SERS). These well-developed single-molecule techniques have been applied to electrochemistry by studying molecules that undergo some characteristic change in an optical property upon redox reaction, enabling the optical readout of electrochemical processes on a single-molecule level. In the most common scheme, a redox molecule will change fluorescence state (i.e., on to off or vice versa) upon electron transfer, thereby transferring the faradaic signal to the optical domain. Under appropriate conditions, this can be observed at the single-molecule level using standard fluorescence microscopy methods. A key difference between this type of detection and electrical detection via redox cycling is that the electrical signal from redox cycling is necessarily the average of many electron transfers (1.6 fA $\approx$ 10,000 electrons/s). Optical detection, on the other hand, enables detection at the single electron transfer level, thereby taking single-molecule electrochemistry to its ultimate limit. Another advantage of optical detection is that it inherently couples the use of microscopy to electrochemistry, bringing the full suite of optical microscopy tools (including subdiffraction limit super-resolution techniques) to electrochemistry. This gives optical detection methods the ability to image reactions and provides for superior spatial resolution opportunities compared to purely electrical detection, where the spatial resolution is determined by electrode size.

Much of the early work in optical detection of single-molecule electrochemistry has been reviewed in detail elsewhere and will only be briefly mentioned here.[134,122] The coupling of fluorescence state (i.e., on or off) to redox state (i.e., oxidized or reduced) was first utilized to study single-molecule electrochemistry by the groups of Bard and Barbara.[135,136] While these studies looked at the coupled electrochemical and fluorescence behavior of a conjugated polymer, the technique was soon demonstrated on small molecules by Ackerman and co-workers.[137,138] In an elegant display of how optical detection can give valuable spatial information, the Chen group used super-resolution microscopy to image the electrocatalytic reaction of single fluorogenic redox molecules on single-walled carbon nanotubes to reveal a heterogeneity in reactive sites along a single nanotube.[139] This proved to be a robust method that has been extended to imaging catalytic heterogeneity in many types of nanocatalysts.[140]

In more recent work, Pan and co-workers studied the single-molecule spectroelectrochemistry of a BODIPY dye that could be driven to an off fluorescence state via irreversible oxidation.[141] They found that embedding the dye molecule in a polystyrene matrix helped preserve photostability and that the dye exhibited a heterogeneous half redox potential distribution of 1.78 ($\pm$0.19) V vs NHE. Through a single-molecule blinking study, the authors were able to determine that dye molecules self-assembled onto nanostructured TiO_2 exhibited fluorescence with the shortest "on" duration time as compared to the dye on glass or ITO substrates. This effect was attributed to a high interfacial charge transfer rate between the dye and TiO_2 surface.

The Bohn group has recently taken a very interesting approach to studying single-molecule spectroelectrochemistry in which they utilize zero-mode waveguides (ZMWs), a concept developed by Craighead and coworkers,[142,143] to

DOI: 10.1021/acs.analchem.5b04542
Anal. Chem. 2016, 88, 414−430

isolate single molecules and perform electrochemistry on them.[144,145] The ZMWs used consist of nanopores with a diameter from ∼20 to 150 nm created by focused ion beam (FIB) milling through a thin Au layer (thickness ≤100 nm) on a fused silica coverslip. Each nanopore serves as a zeptoliter-scale volume to confine the optical signal and isolate single molecules, while the Au nanopore walls serve as a working electrode. In their first report on this method, the group studied the potential-dependent blinking behavior of single flavin adenine dinucleotide (FAD) molecules that were immobilized in ZMWs via a pyrroloquinoline quinone linker.[144] The immobilization procedure was optimized to favor single FAD occupancy in each ZMW. FAD is highly fluorescent in its oxidized state and dark in its reduced state, enabling fluorescent detection of single electron transfer events. From intensity distributions compiled of many single molecules, it was found that, at oxidizing potentials, most molecules were fluorescent, while at reducing potentials, most molecules were non-fluorescent. At potentials near the equilibrium potential, there was a distribution between the two states, with the transition rate between the two states reaching a maximum.

In their most recent study, the Bohn group used ZMWs to study the potential-dependent behavior of freely diffusing single flavin mononucleotide (FMN) molecules.[145] As with FAD, FMN is fluorescent in the oxidized state and nonfluorescent in the reduced state. By carefully choosing the bulk concentration, the average occupancy of each ZMW could be adjusted to the single-molecule level. As with the FAD study, it was found that the probability of observing single FMD molecules in the oxidized state increased as the potential was increased above the equilibrium potential and that the probability of observing single FMD molecules in the reduced state was increased as the potential was decreased below the equilibrium potential. By doing cyclic voltammetry experiments at slow scan rates, the authors observed intermediate fluorescent states that they believe may indicate the presence of an intermediate radical species that is stabilized by the unique environment of the ZMW. Overall, ZMWs represent an exciting and promising new experimental platform for the optical detection of single-molecule electrochemistry.

Fluorescence has also been used to study the single-molecule redox behavior of redox-active proteins, albeit with a slightly modified scheme relying on fluorescent labeling of the protein to form a Förster resonance energy transfer (FRET) donor−acceptor pair.[146,147] In this scheme, a protein that has a redox state dependent absorption band is labeled with a fluorescent dye possessing spectral overlap with the protein. When the protein is in the redox state that favors absorption, part of the excited state energy of the fluorophore is transferred via FRET to the protein, thereby quenching fluorescence. If the protein changes to a redox state that diminishes absorption, FRET decreases, and the fluorescence is enhanced. This method has been used to study the electrochemical behavior of azurin, a metalloprotein with a redox-active Cu ion center that has a strong absorption band at ∼600 nm in the oxidized state that disappears in the reduced state. Initial studies[148−150] succeeded in monitoring azurin immobilized on self-assembled monolayer (SAM)-coated Au thin-film electrodes down to levels of hundreds of molecules and found that, across the electrode surface, the midpoint potential varied by tens of millivolts and the electron transfer rate constant varied by over a factor of 100.[149] Two recent studies have brought detection down to the single azurin molecule level.[151,152] In one report, the redox switching of azurin immobilized on a modified glass surface was studied by varying the chemical potential of the solution,[151] while the other studied azurin immobilized on a SAM-coated Au thin-film electrode under direct voltage control.[152] Both studies again showed dispersion in the thermodynamic midpoint potentials of single azurin molecules.

Optical Detection via Raman Scattering. Due to its exceptionally high sensitivity, SERS has also been used as an optical detection method for single-molecule electrochemistry. This is an exciting method, as it opens up optical single-molecule electrochemistry to nonfluorophore analytes. For SERS detection, the only requirement is that the analyte must undergo a measurable change in its Raman spectrum upon oxidation or reduction. Cortés et al. first reported monitoring the electrochemical response of single Nile blue molecules on Ag colloids by monitoring the Raman band at ∼590 cm^{-1}, which was present in the oxidized state but disappeared in the reduced state.[153] In a follow-up study, the group used increased spectral and temporal resolution to determine that the molecular configuration of individual Nile blue molecules with respect to an Ag nanoparticle surface could alter the charge transfer process, explaining the heterogeneity in single-molecule signals.[154] The group argued that a shorter distance between the molecule and nanoparticle favored charge transfer, resulting in both a less negative reduction potential and smaller Raman frequencies.

In a method analogous to the fluorescence imaging done by the Chen group,[140] the Willets group has recently applied single-molecule super-resolution SERS imaging[155,156] to the subdiffraction limit imaging of redox activity on plasmonic nanoparticles.[157−159] Using superlocalization microscopy, the relative location of a single emitter, or the intensity-weighted superposition of several emitters, can be localized with 5−10 nm precision. Using this method, the Willets group was able to demonstrate that Nile blue molecules exhibit varying redox potentials that depend upon their location on a plasmonic Ag nanoparticle electrode.[158] They then used electrochemical potential modulation to switch Nile blue molecules between the emissive and nonemissive state, enabling the spatial isolation of single molecules at concentrations above the single-molecule level.[158] This effect was used to map out the SERS-active regions on plasmonic nanoparticle aggregates with subdiffraction limit resolution. Their latest study involves using similar methods, while also correlating the resultant super-resolution SERS images with SEM images.[159] This work revealed that Nile blue molecules residing in nanoparticle junctions undergo oxidation and reduction at more negative potentials.

A very recent study reported the coupling of electrochemistry with tip-enhanced Raman spectroscopy (TERS).[160] In TERS, a single Raman "hot spot" is defined by an Au or Ag tip that is controlled by scanning probe microscopy. An electrochemical TERS setup was created by introducing the Raman optical path horizontally to a scanning tunneling microscope (STM) liquid cell. The potential of the tip and substrate were controlled by a bipotentiostat, enabling electrochemical measurements to be made simultaneously with TERS interrogation. Using this setup, the authors studied (4′-(pyridin-4-yl)biphenyl-4-yl)-methanethiol (4-PBT) adsorbed onto an Au(111) substrate. A potential-dependent configuration change of 4-PBT was observed that was consistent with protonation/deprotonation of the molecule. It was estimated that <600 molecules were detected. As TERS has been previously demonstrated to be

DOI: 10.1021/acs.analchem.5b04542
Anal. Chem. 2016, 88, 414−430

capable of single-molecule sensitivity and submolecular spatial resolution,[161] this study represents an exciting first step in coupling electrochemistry to this high-performance optical detection technique.

PROBE-BASED NANOSCALE ELECTROCHEMICAL IMAGING

The nanoscale heterogeneity of interfaces is of great interest in many areas of chemistry and biology, including heterogeneous catalysis, molecular transport at membranes, and corrosion inhibition. Many of these interfaces can be characterized beyond the diffraction limit of conventional optical methods, either with scanning probe techniques such as STM and AFM or with electron microscopy. However, these techniques have not been well-suited for studying the electrochemical heterogeneity of an interface. Researchers have addressed this need, developing analogous scanning probe techniques with the capability of measuring electrochemical heterogeneity. Significant advances have been made in recent years in advancing the imaging capability of these various techniques into the nanoscale spatial resolution regime.

Scanning Electrochemical Microscopy. SECM, a method developed by the Bard lab 27 years ago,[162] has proved to be extremely valuable for a diverse array of electrochemical imaging applications. The technique positions a micro- or nanoelectrode probe in close proximity to an interface of interest and scans the probe over the interface to collect spatially resolved electrochemical information pertaining to it. Generally, the method is used to map out the electrochemical activity of a given interface. SECM has become a well-established technique, and we refer interested readers to a review[163] and monograph[164] on the subject for the basics of the technique as well as previous applications.

When used with nanoelectrode probes, SECM can yield electrochemical information with nanoscale spatial resolution. A recent example of this comes from the Mirkin group, who used Pt nanoelectrodes down to 3 nm in radius to image individual 10 and 20 nm Au nanoparticles on an insulated highly oriented pyrolytic graphite (HOPG) surface.[165] The group reported imaging the particles with unprecedentedly high spatial resolution using ferrocenemethanol as a redox mediator in feedback mode, as well as studying the hydrogen evolution reaction (HER) at individual nanoparticles using substrate generation/tip collection mode. This report was followed up by one in which the group developed the SECM theory for their experimental method of approaching a disk nanoelectrode to a surface-bound spherical nanoparticle.[166]

Due to the scanning nature of SECM, shrinking the size of the probe to get increased spatial resolution means that imaging a given area takes more time as the probe gets smaller. However, minimization of scan times is highly desired to avoid changes to the substrate, probe, and working solution, in addition to avoiding instrument drift and environmental changes (i.e., temperature). Toward that end, Mauzeroll and co-workers examined the change in measured current as a function of probe electrode velocity as a probe approaches a substrate in addition to the contributions arising from the probe angle, both of which can lead to convective contributions to the current.[167] Similarly, the velocity with which a probe electrode is scanned across a surface can impart convective effects, but deconvolution of the measured current can be used to separate out this contribution and enable higher scan speeds to be used.[168] Kiss and Nagy have also shown that aligning the scan pattern with the symmetry of the sample can reduce image distortions and enable higher scan speeds.[169] Most recently, Unwin and co-workers reported developing a high-speed electrochemical imaging platform capable of producing images with a pixel density of 1000 pixels/μm^2 at just over 4 s per frame by measuring up to 8000 pixels/s, representing an improvement in imaging speed of 3−4 orders of magnitude over typical methods.[170] Although this system was developed using SECCM, it should be applicable to SECM as well. This is a very exciting development, as decreasing the imaging time not only avoids the aforementioned experimental problems but also enables the imaging of dynamic processes.

Perhaps the greatest challenge in nanoscale SECM imaging is maintaining a small distance between the probe electrode and substrate. This distance must typically be on the order of magnitude of the diameter of the electroactive portion of the probe. As the electrochemical measurement can be greatly influenced by the probe−substrate distance, it is ideal for this distance to remain fixed throughout a scan. This means that substrates with significant surface roughness require a positional feedback mechanism to ensure that the probe−substrate distance remains fixed throughout the scan. While this has presented experimental challenges, it is ultimately proving beneficial, as researchers have developed various feedback mechanisms that can be harnessed to give high-resolution topographical information. This has enabled methods capable of simultaneously imaging the topography and electrochemical heterogeneity of interfaces with nanoscale spatial resolution. The development of these techniques has been the subject of two excellent recent reviews, which we refer readers to for information beyond what is presented here, such as shear-force SECM.[171,172]

Dual-Function Probe Techniques. A common way to get simultaneous topographical and electrochemical information is to use a dual-function probe technique, which combines either AFM or scanning ion conductance microscopy (SICM) with SECM. In AFM-SECM, which was first reported by Macpherson and Unwin, a specialized nanoelectrode probe is used for both electrochemical and force measurements.[173] A recent report utilizing this technique showed simultaneous topographical and electrochemical mapping of individual 20 nm Au nanoparticles that were functionalized with ferrocene-modified polyethylene glycol (Fc-PEG) groups.[174] Binding the redox mediator to the nanoparticles enabled high resolution electrochemical imaging of the nanoparticles and the grafting density of PEG to be determined on a single-particle basis. In an exciting follow-up study, this strategy was extended to a biological system with the demonstration of imaging Fc-PEG-modified proteins bound to single virus particles.[175] Despite the promise of the technique, the high cost and difficulty of making suitable probes for AFM-SECM have inhibited the technique from widespread adoption. However, progress is being made in remedying this, as evidenced in a recent report describing a batch-fabricated AFM-SECM probe (Figure 7A).[176]

SECM-SICM, first introduced by Korchev and Matsue[177] and Hersam,[178] is a dual-function probe technique that is deservedly receiving increased attention. The technique seems to be a natural union, combining the topographical imaging capabilities of SICM with the electrochemical imaging capabilities of SECM. We note that SICM as a stand-alone technique is developing into an excellent tool for mapping interfaces with nanoscale spatial resolution. However, it will not

DOI: 10.1021/acs.analchem.5b04542
Anal. Chem. 2016, 88, 414−430

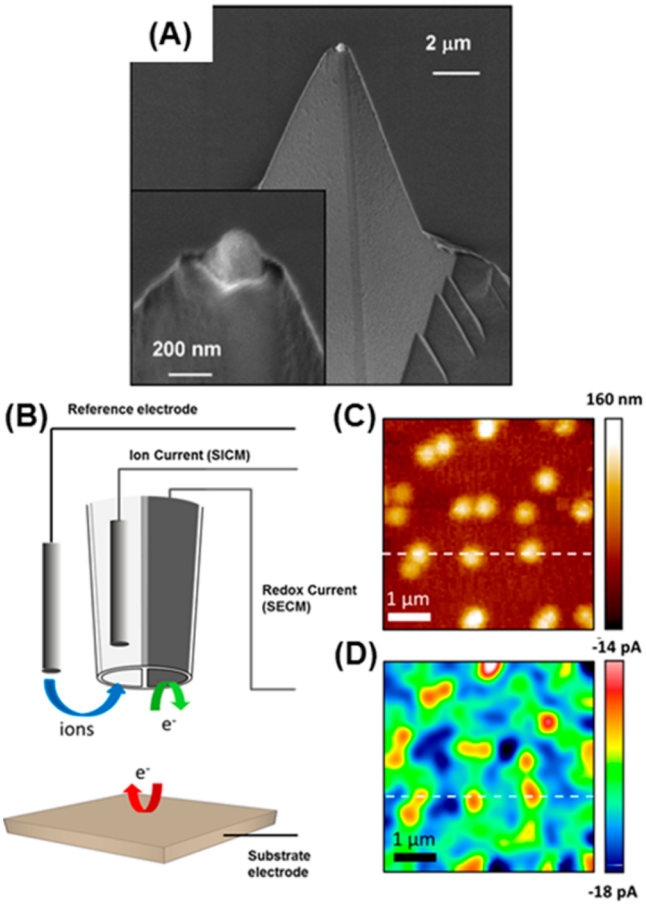

Figure 7. Examples of dual-function probe electrochemical imaging methods. (A) SEM image of a batch-fabricated AFM-SECM tip probe. Reproduced from Wain, A. J.; Pollard, A. J.; Richter, C. *Anal. Chem.* **2014**, *86*, 5143−5149 (ref 176). Copyright 2014 American Chemical Society. (B−D) SECM-SICM imaging of Pt nanospheres. (B) Experimental imaging scheme. (C) Topographic image recorded via SICM. (D) SECM image of competitive oxygen reduction. (C) and (D) were recorded simultaneously. Reproduced from O'Connell, M. A.; Wain, A. J. *Anal. Chem.* **2014**, *86*, 12100−12107 (ref 19). Copyright 2014 American Chemical Society.

be explicitly discussed here, so we refer readers to a recent review on the technique.[179]

In a recent report, O'Connell and Wain used SECM-SICM to map the topography and electrochemical activity of features in the 100−150 nm range.[19] They imaged both an array of Au nanodisks and Pt nanospheres, being able to image the electrochemical activity of individual Pt nanospheres via the oxygen reduction reaction (ORR) (Figure 7B−D). More recently, O'Connell and co-workers used a similar strategy to image individual catalytic Au nanoparticles within an ensemble. Heterogeneous nanoparticles of around 250 nm were deposited onto a glassy carbon substrate, and the topography of individual particles was measured using the SICM channel, while electrochemical mapping was done using the SECM channel. SECM imaging was done in substrate generation/tip collection mode by measuring hydrogen peroxide generated via the ORR at the nanoparticle substrate.[180] The Unwin group used an iridium oxide-modified probe to adapt the method for high resolution pH mapping, which they demonstrated by imaging the topography and pH of a calcite microcrystal during dissolution.[18] SECM-SICM can also be used on biological samples, with a recent example from Şen et al. using a Pt-modified probe to study epidermal growth factor receptors on the membrane of A431 cells.[181] An interesting variation on this technique developed by the Baker group, termed potentiometric-SICM (P-SICM), utilizes a dual-barrel open pipet, with one barrel providing SICM measurements and the other measuring the potential at the tip of the pipet.[182] Using this technique, the group imaged paracellular ion transport across epithelial cells with subcellular spatial resolution.[183]

Scanning Electrochemical Cell Microscopy. Another exciting emerging variation of SECM is scanning electrochemical cell microscopy (SECCM), a method that has been extensively developed by the Unwin group in recent years. We refer readers to a review by the group for the details of the method and an account of its early development.[114] SECCM is a droplet-based technique that typically utilizes a dual-barrel theta pipet with a tip of micrometer to nanometer size (Figure 8A). The barrels of the pipet are filled with electrolyte solution, which forms a small droplet at the end of the tip. This droplet, which is roughly equivalent in size to the tip, is then brought into contact with the substrate of interest for imaging. Ionic current between the pipet barrels can be monitored, providing a mechanism for positional feedback, and the tip can be biased with respect to the substrate, turning the substrate into a working electrode with an area defined by the contact area of the droplet. As such, SECCM is capable of providing coupled high-resolution electrochemical and topographical information. Several recent studies from the Unwin group highlight the utility of this method for nanoscale electrochemical imaging. These studies include imaging the electrochemical activity of: individual carbon nanotubes,[184,185] the basal plane versus step edges of HOPG,[186−188] polycrystalline platinum electrodes,[189−191] photoelectrochemical materials,[192,193] and a cathodic material for Li-ion batteries[194] (Figure 8B−D). This latter study performed simultaneous topographical imaging as well. SECCM has also proven useful for nonimaging applications, including modifying surfaces with high spatial control,[181] studying nanoparticle dynamics,[196,116,117] and by using a modified quad-barrel setup, detecting single redox molecules.[21] The extensive range of applications found for this technique has quickly made SECCM a powerful tool for nanoscale electrochemistry studies.

IN SITU TRANSMISSION ELECTRON MICROSCOPY

A very exciting emerging technique for studying electrochemical processes at the nanoscale is *in situ* electrochemical TEM. Spurred on by the development of liquid-cell TEM sample holders, which enable liquids to be introduced into the high vacuum environment inside a transmission electron microscope, this method makes possible the nanoscale imaging of electrochemical processes under dynamic operating conditions. This technique presents a bit of a twist on the topic of "nanoscale electrochemistry." While the field is usually concerned with studying nanoelectrodes/pores/particles and using them for probing and doing useful things at the nanoscale, *in situ* electrochemical TEM is concerned with imaging electrochemical processes with nanoscale spatial resolution, independent of electrode size. Thus, the technique is "nanoscale electrochemistry" in terms of providing nanoscale-resolution spatial information on electrochemical processes, not necessarily in terms of utilizing nanoscale electrochemical probes.

DOI: 10.1021/acs.analchem.5b04542
Anal. Chem. 2016, 88, 414−430

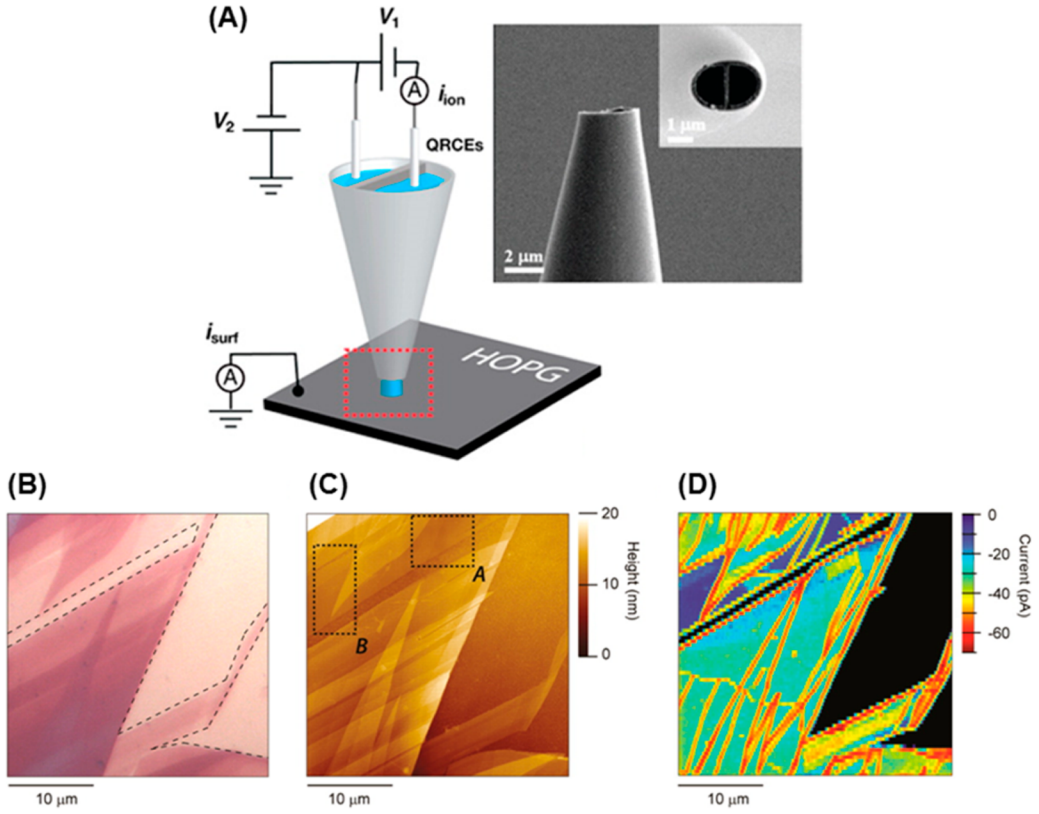

Figure 8. Electrochemical imaging with SECCM. (A) Scheme of an SECCM experiment and SEM image of a micrometer-sized probe tip. Reproduced from Kang, M.; Perry, D.; Kim, Y. R.; Colburn, A. W.; Lazenby, R. A.; Unwin, P. R. *J. Am. Chem. Soc.* **2015**, *137*, 10902−10905. (ref 116). Copyright 2015 American Chemical Society. (B−D) Multimicroscopy of exfoliated graphene (from ZYA grade HOPG) on a Si/SiO_2 substrate. (B) Optical microscopy image (dashed lines define the boundaries between the graphene sample and Si/SiO_2 substrate), (C) AFM topographical image, and (D) SECCM electrochemical map for the reduction of $Ru(NH_3)_6^{3+}$. Reproduced from Güell, A. G.; Cuharuc, A. S.; Kim, Y.-R.; Zhang, G.; Tan, S.-Y.; Ebejer, N.; Unwin, P. R. *ACS Nano* **2015**, *9*, 3558−3571 (ref 188). Copyright 2015 American Chemical Society.

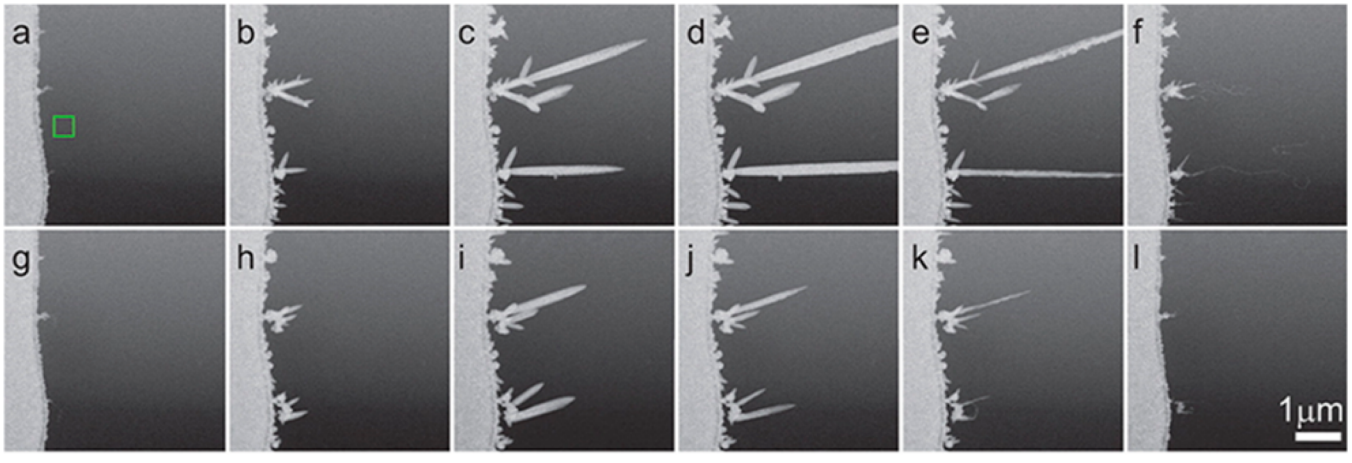

Figure 9. *In situ* TEM imaging of lead dendrite growth and collapse as a working electrode in a solution of lead(II) nitrate is alternately stepped between −1.3 V (b, c, d, h, i) and +0.3 V (a, e, f, g, j, k, l). Reproduced from White, E. R.; Singer, S. B.; Augustyn, V.; Hubbard, W. A.; Mecklenburg, M.; Dunn, B.; Regan, B. C. *ACS Nano* **2012**, *6*, 6308−6317 (ref 211). Copyright 2012 American Chemical Society.

In situ TEM has received an increasing amount of attention during the past several years, and several recent reviews on the subject have appeared in the literature.[197−200] Because of this, we will only briefly highlight some recent advances that are especially relevant to electrochemistry, and we refer the interested reader to these reviews for a more thorough overview of the field. Much of the work utilizing *in situ* electrochemical TEM has focused on studying lithium ion batteries, with a recent focus on using liquid cells for the *operando* study of lithiation/delithiation, formation and morphology of the solid-electrolyte interface (SEI), and lithium electrodeposition.[201−208] *In situ* electrochemical TEM has also been applied to the electrodeposition process of other materials, imaging the dynamic growth of copper,[209] nickel,[210] lead,[211] and most recently, an organic conjugated polymer, poly(3,4-ethylenedioxythiophene) (PEDOT)[212] (Figure 9).

DOI: 10.1021/acs.analchem.5b04542
Anal. Chem. 2016, 88, 414−430

Two recent studies bode well for the future usefulness of the technique. In one, the authors demonstrated for the first time quantitative electrochemical measurements taken using an *in situ* TEM electrochemical liquid cell.[213] The microfluidic cell contained a glassy carbon microelectrode and platinum working and counter electrodes. Using the ferro/ferricyanide redox couple, the authors demonstrated quantitative cyclic voltammetry, chronoamperometry, and electrochemical impedance spectroscopy measurements, thus establishing a foundation for future work concerned with simultaneous quantitative electrochemical measurements and TEM imaging. In the other recent study, the authors used molecular dynamics and image simulations to investigate the possibility of directly imaging the electrical double layer using *in situ* electrochemical TEM.[214] The authors concluded that, for a high-contrast electrolyte such as CsCl and a smooth electrode−electrolyte interface, ion concentration profiles within the double layer should be visible to TEM. This is no doubt an intriguing result that highlights the potential of successfully applying the subnanoscale spatial resolution of TEM to dynamic electrochemical processes.

■ PERSPECTIVES

Nanoscale electrochemistry continues to be one of the most exciting directions in modern electrochemistry research. The use of advanced tools and methods from other areas has brought in enormous new opportunities to this field. We have seen rapid growth of several new and exciting directions in this area including the development and use of more sophisticated, multifunctional nanoelectrode probes, the study of stochastic redox events at the electrode/solution interface, the study of single redox molecules with increased use of microscopic and spectroscopic tools, and the use of liquid cells *in situ* TEM under high vacuum conditions for probing electrochemical processes in real time under reaction conditions. We anticipate that we will continue to see a rapid increase in publications on stochastic electrochemistry of single molecules, nanoparticles, and even biologic cells. The increased use of single-molecule fluorescence microscopy, SERS, and *in situ* TEM will likely bring new information to our study of the electrode/solution interface.

■ AUTHOR INFORMATION

Corresponding Author

*E-mail: zhang@chem.washington.edu. Tel: 206-543-1767. Fax: 206-685-8665.

Notes

The authors declare no competing financial interest.

Biographies

Stephen M. Oja received his B.S. in chemistry from the University of Wisconsin-Madison in 2012. He began his Ph.D. studies that same year at the University of Washington, joining Professor Bo Zhang's lab. His current research interests include developing new electrochemical techniques for imaging and single-molecule detection.

Yunshan Fan received her B.S. in polymer materials science & engineering from Beijing Institute of Technology (China) in 2013. She is currently a Ph.D. student in Professor Bo Zhang's lab at the University of Washington and is investigating electrocatalysis at single nanoparticles using new electrochemical methods.

Chadd M. Armstrong obtained a B.S. in chemistry from Oregon State University in 2014 and continued his studies at the University of Washington immediately following, joining Professor Bo Zhang's lab in 2015. Current research topics of interest include electrochemical scanning probe techniques of nanoscale particles and interfaces.

Peter Defnet received his B.S. in chemistry from Juniata College in 2015. He is currently a graduate student in Professor Bo Zhang's lab at the University of Washington, where he will begin investigating nanopores and electrochemical coupling.

Bo Zhang is an Associate Professor of Chemistry at the University of Washington. He finished his Ph.D. training with Henry White at the University of Utah in 2006 followed by his postdoctoral work with Andrew Ewing at Penn State before joining the UW in 2008. His research at the UW is focused on the development and use of new electrochemical and microscopy methods to better understand chemical reactions at the electrode/solution interface and neuronal communication in the brain. His group has developed the method of fluorescence-enabled electrochemical microscopy (FEEM), which enables fast and high-resolution imaging with very large electrochemical arrays containing millions of nanoelectrodes.

■ ACKNOWLEDGMENTS

We are grateful for financial support from the National Institutes of Health (GM101133), the AFOSR MURI (FA9550-14-1-0003), and the U.S. Defense Threat Reduction Agency (Contract No. HDTRA1-11-1-0005).

■ REFERENCES

(1) Oja, S. M.; Wood, M.; Zhang, B. *Anal. Chem.* **2013**, *85*, 473−476.
(2) Wightman, R. M. *Anal. Chem.* **1981**, *53*, 1125A−1134A.
(3) Murray, R. W. *Chem. Rev.* **2008**, *108*, 2688−2720.
(4) Shen, M.; Colombo, M. L. *Anal. Methods* **2015**, *7*, 7095−7105.
(5) Sun, P.; Mirkin, M. V. *Anal. Chem.* **2006**, *78*, 6526−6534.
(6) Chen, S.; Kucernak, A. *J. Phys. Chem. B* **2003**, *107*, 8392−8402.
(7) Laforge, F. O.; Velmurugan, J.; Wang, Y.; Mirkin, M. V. *Anal. Chem.* **2009**, *81*, 3143−3150.
(8) Fan, F. -R. F.; Bard, A. J. *Science* **1995**, *267*, 871−874.
(9) Chen, S.; Liu, Y. *Phys. Chem. Chem. Phys.* **2014**, *16*, 635−652.
(10) Bond, A. M.; Fleischmann, M.; Robinson, J. *J. Electroanal. Chem. Interfacial Electrochem.* **1984**, *168*, 299−312.
(11) Wehmeyer, K. R.; Deakin, M. R.; Wightman, R. M. *Anal. Chem.* **1985**, *57*, 1913−1916.
(12) Cox, J. T.; Zhang, B. *Annu. Rev. Anal. Chem.* **2012**, *5*, 253−272.
(13) Zoski, C. G. *Electroanalysis* **2002**, *14*, 1041−1051.
(14) Arrigan, D. W. M. *Analyst* **2004**, *129*, 1157−1165.
(15) Kim, J.; Kim, B.-K.; Cho, S. K.; Bard, A. J. *J. Am. Chem. Soc.* **2014**, *136*, 8173−8176.
(16) Liu, Y.; Li, M.; Zhang, F.; Zhu, A.; Shi, G. *Anal. Chem.* **2015**, *87*, 5531−5538.
(17) Takahashi, Y.; Shevchuk, A. I.; Novak, P.; Zhang, Y.; Ebejer, N.; Macpherson, J. V.; Unwin, P. R.; Pollard, A. J.; Roy, D.; Clifford, C. A.; Shiku, H.; Matsue, T.; Klenerman, D.; Korchev, Y. E. *Angew. Chem., Int. Ed.* **2011**, *50*, 9638−9642.
(18) Nadappuram, B. P.; McKelvey, K.; Al Botros, R.; Colburn, A. W.; Unwin, P. R. *Anal. Chem.* **2013**, *85*, 8070−8074.
(19) O'Connell, M. A.; Wain, A. J. *Anal. Chem.* **2014**, *86*, 12100−12107.
(20) Paulose Nadappuram, B.; McKelvey, K.; Byers, J. C.; Güell, A. G.; Colburn, A. W.; Lazenby, R. A.; Unwin, P. R. *Anal. Chem.* **2015**, *87*, 3566−3573.
(21) Byers, J. C.; Paulose Nadappuram, B.; Perry, D.; McKelvey, K.; Colburn, A. W.; Unwin, P. R. *Anal. Chem.* **2015**, *87*, 10450−10456.
(22) Actis, P.; Tokar, S.; Clausmeyer, J.; Babakinejad, B.; Mikhaleva, S.; Cornut, R.; Takahashi, Y.; Córdoba, A. L.; Novak, P.; Shevchuck, A. I.; Dougan, J. A.; Kazarian, S. G.; Gorelkin, P. V.; Erofeev, A. S.; Yaminsky, I. V.; Unwin, P. R.; Schuhmann, W.; Klenerman, D.; Rusakov, D. A.; Sviderskaya, E. V.; Korchev, Y. E. *ACS Nano* **2014**, *8*, 875−884.

DOI: 10.1021/acs.analchem.5b04542
Anal. Chem. 2016, 88, 414−430

(23) Yu, Y.; Noël, J.-M.; Mirkin, M. V.; Gao, Y.; Mashtalir, O.; Friedman, G.; Gogotsi, Y. *Anal. Chem.* **2014**, *86*, 3365−3372.
(24) Yu, Y.; Gao, Y.; Hu, K.; Blanchard, P.-Y.; Noël, J.-M.; Nareshkumar, T.; Phani, K. L.; Friedman, G.; Gogotsi, Y.; Mirkin, M. V. *ChemElectroChem* **2015**, *2*, 58−63.
(25) Nioradze, N.; Chen, R.; Kim, J.; Shen, M.; Santhosh, P.; Amemiya, S. *Anal. Chem.* **2013**, *85*, 6198−6202.
(26) Bard, A. J.; Faulkner, L. R. *Electrochemical Methods*, 2nd ed.; John Wiley & Sons: New York, 2001; Chapter 5.
(27) Ellison, J.; Eloul, S.; Batchelor-McAuley, C.; Tschulik, K.; Salter, C.; Compton, R. G. *J. Electroanal. Chem.* **2015**, *745*, 66−71.
(28) Renault, C.; Marchuk, K.; Ahn, H. S.; Titus, E. J.; Kim, J.; Willets, K. A.; Bard, A. J. *Anal. Chem.* **2015**, *87*, 5730−5737.
(29) Sun, T.; Blanchard, P.-Y.; Mirkin, M. V. *Anal. Chem.* **2015**, *87*, 4092−4095.
(30) Coulter, W. H. *Means for Counting Particles Suspended in a Fluid*. US Patent No. 2656508, 1953.
(31) Wang, G.; Wang, L.; Han, Y.; Zhou, S.; Guan, X. *Acc. Chem. Res.* **2013**, *46*, 2867−2877.
(32) Ito, T.; Sun, L.; Crooks, R. M. *Anal. Chem.* **2003**, *75*, 2399−2406.
(33) Venta, K. E.; Zanjani, M. B.; Ye, X.; Danda, G.; Murray, C. B.; Lukes, J. R.; Drndic, M. *Nano Lett.* **2014**, *14*, 5358−5364.
(34) Qiu, Y.; Yang, C.; Hinkle, P.; Vlassiouk, I. V.; Siwy, Z. S. *Anal. Chem.* **2015**, *87*, 8517−8523.
(35) Manrao, E. A.; Derrington, I. M.; Laszlo, A. H.; Langford, K. W.; Hopper, M. K.; Gillgren, N.; Pavlenok, M.; Niederweis, M.; Gundlach, J. H. *Nat. Biotechnol.* **2012**, *30*, 349−354.
(36) Ayub, M.; Bayley, H. *Nano Lett.* **2012**, *12*, 5637−5643.
(37) Li, W.; Gong, L.; Bayley, H. *Angew. Chem., Int. Ed.* **2013**, *52*, 4350−4355.
(38) Perera, R. T.; Fleming, A. M.; Johnson, R. P.; Burrows, C. J.; White, H. S. *Nanotechnology* **2015**, *26*, 074002.
(39) An, N.; Fleming, A. M.; White, H. S.; Burrows, C. *ACS Nano* **2015**, *9*, 4296−4307.
(40) Movileanu, L. *Soft Matter* **2008**, *4*, 925−931.
(41) Harms, Z. D.; Mogensen, K. B.; Nunes, P. S.; Zhou, K.; Hildenbrand, B. W.; Mitra, I.; Tan, Z.; Zlotnick, A.; Kutter, J. P.; Jacobson, S. C. *Anal. Chem.* **2011**, *83*, 9573−9578.
(42) Zhou, K.; Li, L.; Tan, Z.; Zlotnick, A.; Jacobson, S. C. *J. Am. Chem. Soc.* **2011**, *133*, 1618−1621.
(43) Li, G.; Zhang, Z.; Lin, X. *Chin. J. Anal. Chem.* **2010**, *38*, 1698−1702.
(44) Heins, E. A.; Siwy, Z. S.; Baker, L. A.; Martin, C. R. *Nano Lett.* **2005**, *5*, 1824−1829.
(45) Berge, L. I.; Feder, J.; Jøssang, T. *Rev. Sci. Instrum.* **1989**, *60*, 2756−2763.
(46) Branton, D.; Deamer, D. W.; Marziali, A.; Bayley, H.; Benner, S. A.; Butler, T.; Di Ventra, M.; Garaj, S.; Hibbs, A.; Huang, X.; Jovanovich, S. B.; Krstic, P. S.; Lindsay, S.; Ling, X. S.; Mastrangelo, C. H.; Meller, A.; Oliver, J. S.; Pershin, Y. V.; Ramsey, J. M.; Riehn, R.; Soni, G. V.; Tabard-Cossa, V.; Wanunu, M.; Wiggin, M.; Schloss, J. A. *Nat. Biotechnol.* **2008**, *26*, 1146−1153.
(47) Feng, Y.; Zhang, Y.; Ying, C.; Wang, D.; Du, C. *Genomics, Proteomics Bioinf.* **2015**, *13*, 4−16.
(48) Kwok, H.; Briggs, K.; Tabard-Cossa, V. *PLoS One* **2014**, *9*, e92880.
(49) Haywood, D. G.; Saha-Shah, A.; Baker, L. A.; Jacobson, S. C. *Anal. Chem.* **2015**, *87*, 172−187.
(50) Li, J.; Stein, D.; McMullan, C.; Branton, D.; Aziz, M. J.; Golovchenko, J. A. *Nature* **2001**, *412*, 166−169.
(51) Storm, A. J.; Chen, J. H.; Ling, X. S.; Zandbergen, H. W.; Dekker, C. *Nat. Mater.* **2003**, *2*, 537−540.
(52) Howorka, S.; Siwy, Z. *Chem. Soc. Rev.* **2009**, *38*, 2360−2384.
(53) Briggs, K.; Kwok, H.; Tabard-Cossa, V. *Small* **2014**, *10*, 2077−2086.
(54) Kowalczyk, S. W.; Grosberg, A. Y.; Rabin, Y.; Dekker, C. *Nanotechnology* **2011**, *22*, 315101.
(55) Kuan, A. T.; Lu, B.; Xie, P.; Szalay, T.; Golovchenko, J. E. *Appl. Phys. Lett.* **2015**, *106*, 203109.
(56) Kwok, H.; Waugh, M.; Bustamante, J.; Briggs, K.; Tabard-Cossa, V. *Adv. Funct. Mater.* **2014**, *24*, 7745−7753.
(57) Tahvildari, R.; Beamish, E.; Tabard-Cossa, V.; Godin, M. *Lab Chip* **2015**, *15*, 1407−1411.
(58) Briggs, K.; Charron, M.; Kwok, H.; Le, T.; Chahal, S.; Bustamante, J.; Waugh, M.; Tabard-Cossa, V. *Nanotechnology* **2015**, *26*, 084004.
(59) Pud, S.; Verschueren, D.; Vukovic, N.; Plesa, C.; Jonsson, M. P.; Dekker, C. *Nano Lett.* **2015**, *15*, 7112−7117.
(60) Kasianowicz, J. J.; Brandin, E.; Branton, D.; Deamer, D. W. *Proc. Natl. Acad. Sci. U. S. A.* **1996**, *93*, 13770−13773.
(61) Menestrina, G. *J. Membr. Biol.* **1986**, *90*, 177−190.
(62) Gouaux, J. E.; Braha, O.; Hobaugh, M. R.; Song, L.; Cheley, S.; Shustak, C.; Bayley, H. *Proc. Natl. Acad. Sci. U. S. A.* **1994**, *91*, 12828−12831.
(63) Butler, T. Z.; Pavlenok, M.; Derrington, I. M.; Niederweis, M.; Gundlach, J. H. *Proc. Natl. Acad. Sci. U. S. A.* **2008**, *105*, 20647−20652.
(64) Manrao, E. A.; Derrington, I. M.; Pavlenok, M.; Niederweis, M.; Gundlach, J. H. *PLoS One* **2011**, *6*, e25723.
(65) Cracknell, J. A.; Japrung, D.; Bayley, H. *Nano Lett.* **2013**, *13*, 2500−2505.
(66) Clamer, M.; Hofler, L.; Mikhailova, E.; Viero, G.; Bayley, H. *ACS Nano* **2014**, *8*, 1364−1374.
(67) Baaken, G.; Halimeh, I.; Bacri, L.; Pelta, J.; Oukhaled, A.; Behrends, J. C. *ACS Nano* **2015**, *9*, 6443−6449.
(68) Hernandez-Ainsa, S.; Keyser, U. F. *Nanoscale* **2014**, *6*, 14121−14132.
(69) Rothemund, P. W. K. *Nature* **2006**, *440*, 297−302.
(70) Zhang, F.; Nangreave, J.; Liu, Y.; Yan, H. *J. Am. Chem. Soc.* **2014**, *136*, 11198−11211.
(71) Douglas, S. M.; Marblestone, A. H.; Teerapittayanon, S.; Vazquez, A.; Church, G. M.; Shih, W. M. *Nucleic Acids Res.* **2009**, *37*, 5001−5006.
(72) Jabbari, H.; Aminpour, M.; Montemagno, C. *ACS Comb. Sci.* **2015**, *17*, 535−547.
(73) Hernandez-Ainsa, S.; Misiunas, K.; Thacker, V. V.; Hemmig, E. A.; Keyser, U. F. *Nano Lett.* **2014**, *14*, 1270−1274.
(74) Bell, N. A. W.; Engst, C. R.; Ablay, M.; Divitini, G.; Ducati, C.; Liedl, T.; Keyser, U. F. *Nano Lett.* **2012**, *12*, 512−517.
(75) Gilboa, T.; Meller, A. *Analyst* **2015**, *140*, 4733−4747.
(76) Kleijn, S. E. F.; Lai, S. C. S.; Koper, M. T. M.; Unwin, P. R. *Angew. Chem., Int. Ed.* **2014**, *53*, 3558−3586.
(77) Sambur, J. B.; Chen, P. *Annu. Rev. Phys. Chem.* **2014**, *65*, 395−422.
(78) Wang, W.; Tao, N. *Anal. Chem.* **2014**, *86*, 2−14.
(79) Xiao, X.; Bard, A. J. *J. Am. Chem. Soc.* **2007**, *129*, 9610−9612.
(80) Stuart, E. J. E.; Tschulik, K.; Batchelor-McAuley, C.; Compton, R. G. *ACS Nano* **2014**, *8*, 7648−7654.
(81) Lim, C. S.; Tan, S. M.; Sofer, Z.; Pumera, M. *ACS Nano* **2015**, *9*, 8474−8483.
(82) Fernando, A.; Parajuli, S.; Alpuche-Aviles, M. A. *J. Am. Chem. Soc.* **2013**, *135*, 10894−10897.
(83) Sardesai, N. P.; Andreescu, D.; Andreescu, S. *J. Am. Chem. Soc.* **2013**, *135*, 16770−16773.
(84) Perera, N.; Karunathilake, N.; Chhetri, P.; Alpuche-Aviles, M. A. *Anal. Chem.* **2015**, *87*, 777−784.
(85) Giovanni, M.; Ambrosi, A.; Sofer, Z.; Pumera, M. *Electrochem. Commun.* **2015**, *56*, 16−19.
(86) Kim, B.-K.; Kim, J.; Bard, A. J. *J. Am. Chem. Soc.* **2015**, *137*, 2343−2349.
(87) Kim, B. K.; Boika, A.; Kim, J.; Dick, J. E.; Bard, A. J. *J. Am. Chem. Soc.* **2014**, *136*, 4849−4852.
(88) Li, Y.; Deng, H.; Dick, J. E.; Bard, A. J. *Anal. Chem.* **2015**, *87*, 11013−11021.
(89) Dick, J. E.; Renault, C.; Kim, B.-K.; Bard, A. J. *Angew. Chem., Int. Ed.* **2014**, *53*, 11859−11862.

DOI: 10.1021/acs.analchem.5b04542
Anal. Chem. 2016, 88, 414−430

(90) Cheng, W.; Compton, R. G. *Angew. Chem., Int. Ed.* **2014**, *53*, 13928−13930.
(91) Cheng, W.; Compton, R. G. *Angew. Chem., Int. Ed.* **2015**, *54*, 7082−7085.
(92) Dunevall, J.; Fathali, H.; Najafinobar, N.; Lovric, J.; Wigstrom, J.; Cans, A. S.; Ewing, A. G. *J. Am. Chem. Soc.* **2015**, *137*, 4344−4346.
(93) Toh, H. S.; Compton, R. G. *Chem. Sci.* **2015**, *6*, 5053−5058.
(94) Lebègue, E.; Anderson, C. M.; Dick, J. E.; Webb, L. J.; Bard, A. J. *Langmuir* **2015**, *31*, 11734−11739.
(95) Wakerley, D.; Güell, A. G.; Hutton, L. A.; Miller, T. S.; Bard, A. J.; Macpherson, J. V. *Chem. Commun.* **2013**, *49*, 5657−5659.
(96) Dasari, R.; Robinson, D. A.; Stevenson, K. J. *J. Am. Chem. Soc.* **2013**, *135*, 570−573.
(97) Dasari, R.; Tai, K.; Robinson, D. A.; Stevenson, K. J. *ACS Nano* **2014**, *8*, 4539−4546.
(98) Ahn, H. S.; Bard, A. J. *Angew. Chem., Int. Ed.* **2015**, *54*, 13753−13757.
(99) Fosdick, S. E.; Anderson, M. J.; Nettleton, E. G.; Crooks, R. M. *J. Am. Chem. Soc.* **2013**, *135*, 5994−5997.
(100) Robinson, D. A.; Yoo, J. J.; Castañeda, A. D.; Gu, B.; Dasari, R.; Crooks, R. M.; Stevenson, K. J. *ACS Nano* **2015**, *9*, 7583−7595.
(101) Santos, G. P.; Melo, A. F. A. A.; Crespilho, F. N. *Phys. Chem. Chem. Phys.* **2014**, *16*, 8012−8018.
(102) Yoo, J. J.; Kim, J.; Crooks, R. M. *Chem. Sci.* **2015**, *6*, 6665−6671.
(103) Guo, Z.; Percival, S. J.; Zhang, B. *J. Am. Chem. Soc.* **2014**, *136*, 8879−8882.
(104) Li, Y.; Cox, J. T.; Zhang, B. *J. Am. Chem. Soc.* **2010**, *132*, 3047−3054.
(105) Lakbub, J.; Pouliwe, A.; Kamasah, A.; Yang, C.; Sun, P. *Electroanalysis* **2011**, *23*, 2270−2274.
(106) Sun, P.; Li, F.; Yang, C.; Sun, T.; Kady, I.; Hunt, B.; Zhuang, J. *J. Phys. Chem. C* **2013**, *117*, 6120−6125.
(107) Shan, X.; Patel, U.; Wang, S.; Iglesias, R.; Tao, N. *Science* **2010**, *327*, 1363−1366.
(108) Shan, X.; Diez-Perez, I.; Wang, L.; Wiktor, P.; Gu, Y.; Zhang, L.; Wang, W.; Lu, J.; Wang, S.; Gong, Q.; Li, J.; Tao, N. *Nat. Nanotechnol.* **2012**, *7*, 668−672.
(109) Fang, Y.; Wang, W.; Wo, X.; Luo, Y.; Yin, S.; Wang, Y.; Shan, X.; Tao, N. *J. Am. Chem. Soc.* **2014**, *136*, 12584−12587.
(110) Hill, C. M.; Pan, S. *J. Am. Chem. Soc.* **2013**, *135*, 17250−17253.
(111) Hill, C. M.; Bennett, R.; Zhou, C.; Street, S.; Zheng, J.; Pan, S. *J. Phys. Chem. C* **2015**, *119*, 6760−6768.
(112) Byers, C. P.; Hoener, B. S.; Chang, W.-S.; Yorulmaz, M.; Link, S.; Landes, C. F. *J. Phys. Chem. B* **2014**, *118*, 14047−14055.
(113) Jing, C.; Rawson, F. J.; Zhou, H.; Shi, X.; Li, W.-H.; Li, D.-W.; Long, Y.-T. *Anal. Chem.* **2014**, *86*, 5513−5518.
(114) Ebejer, N.; Güell, A. G.; Lai, S. C. S.; McKelvey, K.; Snowden, M. E.; Unwin, P. R. *Annu. Rev. Anal. Chem.* **2013**, *6*, 329−351.
(115) Kleijn, S. E.; Lai, S. C.; Miller, T. S.; Yanson, A. I.; Koper, M. T.; Unwin, P. R. *J. Am. Chem. Soc.* **2012**, *134*, 18558−18561.
(116) Kang, M.; Perry, D.; Kim, Y. R.; Colburn, A. W.; Lazenby, R. A.; Unwin, P. R. *J. Am. Chem. Soc.* **2015**, *137*, 10902−10905.
(117) Chen, C.-H.; Ravenhill, E. R.; Momotenko, D.; Kim, Y.-R.; Lai, S. C. S.; Unwin, P. R. *Langmuir* **2015**, *31*, 11932−11942.
(118) Moerner, W. E. *Angew. Chem., Int. Ed.* **2015**, *54*, 8067−8093.
(119) Sun, L.; Diaz-Fernandez, Y. A.; Gschneidtner, T. A.; Westerlund, F.; Lara-Avila, S.; Moth-Poulsen, K. *Chem. Soc. Rev.* **2014**, *43*, 7378−7411.
(120) Nichols, R. J.; Higgins, S. J. *Annu. Rev. Anal. Chem.* **2015**, *8*, 389−417.
(121) Lemay, S. G.; Kang, S.; Mathwig, K.; Singh, P. S. *Acc. Chem. Res.* **2013**, *46*, 369−377.
(122) Mathwig, K.; Aartsma, T. J.; Canters, G. W.; Lemay, S. G. *Annu. Rev. Anal. Chem.* **2014**, *7*, 383−404.
(123) Mathwig, K.; Albrecht, T.; Goluch, E. D.; Rassaei, L. *Anal. Chem.* **2015**, *87*, 5470−5475.
(124) Fan, F. -R. F.; Kwak, J.; Bard, A. J. *J. Am. Chem. Soc.* **1996**, *118*, 9669−9675.
(125) Bard, A. J.; Fan, F. -R. F. *Acc. Chem. Res.* **1996**, *29*, 572−578.
(126) Sun, P.; Mirkin, M. V. *J. Am. Chem. Soc.* **2008**, *130*, 8241−8250.
(127) Zevenbergen, M. A. G.; Singh, P. S.; Goluch, E. D.; Wolfrum, B. L.; Lemay, S. G. *Nano Lett.* **2011**, *11*, 2881−2886.
(128) Kang, S.; Nieuwenhuis, A. F.; Mathwig, K.; Mampallil, D.; Lemay, S. G. *ACS Nano* **2013**, *7*, 10931−10937.
(129) Rassaei, L.; Mathwig, K.; Kang, S.; Heering, H. A.; Lemay, S. G. *ACS Nano* **2014**, *8*, 8278−8284.
(130) Mampallil, D.; Mathwig, K.; Kang, S.; Lemay, S. G. *J. Phys. Chem. Lett.* **2014**, *5*, 636−640.
(131) Kätelhön, E.; Krause, K. J.; Mathwig, K.; Lemay, S. G.; Wolfrum, B. *ACS Nano* **2014**, *8*, 4924−4930.
(132) Feldberg, S. W.; Edwards, M. A. *Anal. Chem.* **2015**, *87*, 3778−3783.
(133) Dick, J. E.; Renault, C. R.; Bard, A. J. *J. Am. Chem. Soc.* **2015**, *137*, 8376−8379.
(134) Hill, C. M.; Clayton, D. A.; Pan, S. *Phys. Chem. Chem. Phys.* **2013**, *15*, 20797−20807.
(135) Palacios, R. E.; Fan, F. -R. F.; Bard, A. J.; Barbara, P. F. *J. Am. Chem. Soc.* **2006**, *128*, 9028−9029.
(136) Palacios, R. E.; Fan, F. -R. F.; Grey, J. K.; Suk, J.; Bard, A. J.; Barbara, P. F. *Nat. Mater.* **2007**, *6*, 680−685.
(137) Lei, C.; Hu, D.; Ackerman, E. J. *Chem. Commun.* **2008**, 5490−5492.
(138) Lei, C.; Hu, D.; Ackerman, E. J. *Nano Lett.* **2009**, *9*, 655−658.
(139) Xu, W.; Shen, H.; Kim, Y. J.; Zhou, X.; Liu, G.; Park, J.; Chen, P. *Nano Lett.* **2009**, *9*, 3968−3973.
(140) Chen, P.; Zhou, X.; Andoy, N. M.; Han, K.-S.; Choudhary, E.; Zou, N.; Chen, G.; Shen, H. *Chem. Soc. Rev.* **2014**, *43*, 1107−1117.
(141) Liu, J.; Hill, C. M.; Pan, S.; Liu, H. *Phys. Chem. Chem. Phys.* **2014**, *16*, 23150−23156.
(142) Levene, M. J.; Korlach, J.; Turner, S. W.; Foquet, M.; Craighead, H. G.; Webb, W. W. *Science* **2003**, *299*, 682−686.
(143) Zhu, P.; Craighead, H. G. *Annu. Rev. Biophys.* **2012**, *41*, 269−293.
(144) Zhao, J.; Zaino, L. P., III; Bohn, P. W. *Faraday Discuss.* **2013**, *164*, 57−69.
(145) Zaino, L. P.; Grismer, D. A.; Han, D.; Crouch, G. M.; Bohn, P. W. *Faraday Discuss.* **2015**, DOI: 10.1039/C5FD00072F.
(146) Schmauder, R.; Alagaratnam, S.; Chan, C.; Schmidt, T.; Canters, G. W.; Aartsma, T. J. *JBIC, J. Biol. Inorg. Chem.* **2005**, *10*, 683−687.
(147) Kuznetsova, S.; Zauner, G.; Schmauder, R.; Mayboroda, O. A.; Deelder, A. M.; Aartsma, T. J.; Canters, G. W. *Anal. Biochem.* **2006**, *350*, 52−60.
(148) Davis, J. J.; Burgess, H.; Zauner, G.; Kuznetsova, S.; Salverda, J.; Aartsma, T.; Canters, G. W. *J. Phys. Chem. B* **2006**, *110*, 20649−20654.
(149) Salverda, J. M.; Patil, A. V.; Mizzon, G.; Kuznetsova, S.; Zauner, G.; Akkilic, N.; Canters, G. W.; Davis, J. J.; Heering, H. A.; Aartsma, T. J. *Angew. Chem.* **2010**, *122*, 5912−5915.
(150) Patil, A. V.; Davis, J. J. *J. Am. Chem. Soc.* **2010**, *132*, 16938−16944.
(151) Akkilic, N.; van der Grient, F.; Kamran, M.; Sanghamitra, N. J. M. *Chem. Commun.* **2014**, *50*, 14523−14526.
(152) Akkilic, N.; Kamran, M.; Stan, R.; Sanghamitra, N. J. M. *Biosens. Bioelectron.* **2015**, *67*, 747−751.
(153) Cortés, E.; Etchegoin, P. G.; Le Ru, E. C.; Fainstein, A.; Vela, M. E.; Salvarezza, R. C. *J. Am. Chem. Soc.* **2010**, *132*, 18034−18037.
(154) Cortés, E.; Etchegoin, P. G.; Le Ru, E. C.; Fainstein, A.; Vela, M. E.; Salvarezza, R. C. *J. Am. Chem. Soc.* **2013**, *135*, 2809−2815.
(155) Stranahan, S. M.; Willets, K. A. *Nano Lett.* **2010**, *10*, 3777−3784.
(156) Willets, K. A.; Stranahan, S. M.; Weber, M. L. *J. Phys. Chem. Lett.* **2012**, *3*, 1286−1294.
(157) Wilson, A. J.; Willets, K. A. *Nano Lett.* **2014**, *14*, 939−945.
(158) Willets, K. A.; Weber, M. L. *Proc. SPIE* **2015**, *9467*, 946710.

DOI: 10.1021/acs.analchem.5b04542
Anal. Chem. 2016, 88, 414−430

(159) Weber, M. L.; Wilson, A. J.; Willets, K. A. *J. Phys. Chem. C* **2015**, *119*, 18591−18601.
(160) Zeng, Z.-C.; Huang, S.-C.; Wu, D.-Y.; Meng, L.-Y.; Li, M.-H.; Huang, T.-X.; Zhong, J.-H.; Wang, X.; Yang, Z.-L.; Ren, B. *J. Am. Chem. Soc.* **2015**, *137*, 11928−11931.
(161) Sonntag, M. D.; Pozzi, E. A.; Jiang, N.; Hersam, M. C.; Van Duyne, R. P. *J. Phys. Chem. Lett.* **2014**, *5*, 3125−3130.
(162) Bard, A. J.; Fan, F. -R. F.; Kwak, J.; Lev, O. *Anal. Chem.* **1989**, *61*, 132−138.
(163) Amemiya, S.; Bard, A. J.; Fan, F. -R. F.; Mirkin, M. V.; Unwin, P. R. *Annu. Rev. Anal. Chem.* **2008**, *1*, 95−131.
(164) Bard, A. J., Mirkin, M. V., Eds. *Scanning Electrochemical Microscopy*, 2nd ed.; CRC Press: Boca Raton, FL, 2012.
(165) Sun, T.; Yu, Y.; Zacher, B. J.; Mirkin, M. V. *Angew. Chem., Int. Ed.* **2014**, *53*, 14120−14123.
(166) Yu, Y.; Sun, T.; Mirkin, M. V. *Anal. Chem.* **2015**, *87*, 7446−7453.
(167) Cornut, R.; Poirier, S.; Mauzeroll, J. *Anal. Chem.* **2012**, *84*, 3531−3537.
(168) Kiss, A.; Nagy, G. *Electrochim. Acta* **2015**, *163*, 303−309.
(169) Kiss, A.; Nagy, G. *Electrochim. Acta* **2014**, *119*, 169−174.
(170) Momotenko, D.; Byers, J. C.; McKelvey, K.; Kang, M.; Unwin, P. R. *ACS Nano* **2015**, *9*, 8942−8952.
(171) Kranz, C. *Analyst* **2014**, *139*, 336−352.
(172) O'Connell, M. A.; Wain, A. J. *Anal. Methods* **2015**, *7*, 6983−6999.
(173) Macpherson, J. V.; Unwin, P. R. *Anal. Chem.* **2000**, *72*, 276−285.
(174) Huang, K.; Anne, A.; Bahri, M. A.; Demaille, C. *ACS Nano* **2013**, *7*, 4151−4163.
(175) Nault, L.; Taofifenua, C.; Anne, A.; Chovin, A.; Demaille, C.; Besong-Ndika, J.; Cardinale, D.; Carette, N.; Michon, T.; Walter, J. *ACS Nano* **2015**, *9*, 4911−4924.
(176) Wain, A. J.; Pollard, A. J.; Richter, C. *Anal. Chem.* **2014**, *86*, 5143−5149.
(177) Takahashi, Y.; Shevchuk, A. I.; Novak, P.; Murakami, Y.; Shiku, H.; Korchev, Y. E.; Matsue, T. *J. Am. Chem. Soc.* **2010**, *132*, 10118−10126.
(178) Comstock, D. J.; Elam, J. W.; Pellin, M. J.; Hersam, M. C. *Anal. Chem.* **2010**, *82*, 1270−1276.
(179) Chen, C.-C.; Zhou, Y.; Baker, L. A. *Annu. Rev. Anal. Chem.* **2012**, *5*, 207−228.
(180) O'Connell, M. A.; Lewis, J. R.; Wain, A. J. *Chem. Commun.* **2015**, *51*, 10314−10317.
(181) Şen, M.; Takahashi, Y.; Matsumae, Y.; Horiguchi, Y.; Kumatani, A.; Ino, K.; Shiku, H.; Matsue, T. *Anal. Chem.* **2015**, *87*, 3484−3459.
(182) Zhou, Y.; Chen, C.-C.; Weber, A. E.; Zhou, L.; Baker, L. A. *Langmuir* **2014**, *30*, 5669−5675.
(183) Chen, C.-C.; Zhou, Y.; Morris, C. A.; Hou, J.; Baker, L. A. *Anal. Chem.* **2013**, *85*, 3621−3628.
(184) Güell, A. G.; Meadows, K. E.; Dudin, P. V.; Ebejer, N.; Macpherson, J. V.; Unwin, P. R. *Nano Lett.* **2014**, *14*, 220−224.
(185) Güell, A. G.; Meadows, K. E.; Dudin, P. V.; Ebejer, N.; Byers, J. C.; Macpherson, J. V.; Unwin, P. R. *Faraday Discuss.* **2014**, *172*, 439−455.
(186) Patel, A. N.; Tan, S.-Y.; Unwin, P.R. *Chem. Commun.* **2013**, *49*, 8776−8778.
(187) Zhang, G.; Kirkman, P. M.; Patel, A. N.; Cuharuc, A. S.; McKelvey, K.; Unwin, P. R. *J. Am. Chem. Soc.* **2014**, *136*, 11444−11451.
(188) Güell, A. G.; Cuharuc, A. S.; Kim, Y.-R.; Zhang, G.; Tan, S.-Y.; Ebejer, N.; Unwin, P. R. *ACS Nano* **2015**, *9*, 3558−3571.
(189) Aaronson, B. D. B.; Lai, S. C. S.; Unwin, P. R. *Langmuir* **2014**, *30*, 1915−1919.
(190) Chen, C.-H.; Meadows, K. E.; Cuharuc, A.; Lai, S. C. S.; Unwin, P. R. *Phys. Chem. Chem. Phys.* **2014**, *16*, 18545−18552.
(191) Chen, C.-H.; Jacobse, L.; McKelvey, K.; Lai, S. C. S.; Koper, M. T. M.; Unwin, P. R. *Anal. Chem.* **2015**, *87*, 5782−5789.
(192) Aaronson, B. D. B.; Byers, J. C.; Colburn, A. W.; McKelvey, K.; Unwin, P. R. *Anal. Chem.* **2015**, *87*, 4129−4133.
(193) Aaronson, B. D. B.; Garoz-Ruiz, J.; Byers, J. C.; Colina, A.; Unwin, P. R. *Langmuir* **2015**, *31*, 12814−12822.
(194) Takahashi, Y.; Kumatani, A.; Munakata, H.; Inomata, H.; Ito, K.; Ino, K.; Shiku, H.; Unwin, P. R.; Korchev, Y. E.; Kanamura, K.; Matsue, T. *Nat. Commun.* **2014**, *5*, 5450.
(195) Kirkman, P. M.; Güell, A. G.; Cuharuc, A. S.; Unwin, P. R. *J. Am. Chem. Soc.* **2014**, *136*, 36−39.
(196) Lai, S. C. S.; Lazenby, R. A.; Kirkman, P. M.; Unwin, P. R. *Chem. Sci.* **2015**, *6*, 1126−1138.
(197) Wu, F.; Yao, N. *Nano Energy* **2015**, *11*, 196−210.
(198) Wang, C.-M.; Liao, H.-G.; Ross, F. M. *MRS Bull.* **2015**, *40*, 46−52.
(199) Wang, C.-M. *J. Mater. Res.* **2015**, *30*, 326−339.
(200) Ramachandramoorthy, R.; Bernal, R.; Espinosa, H. D. *ACS Nano* **2015**, *9*, 4675−4685.
(201) Gu, M.; Parent, L. R.; Mehdi, B. L.; Unocic, R. R.; McDowell, M. T.; Sacci, R. L.; Xu, W.; Connell, J. G.; Xu, P.; Abellan, P.; Chen, X.; Zhang, Y.; Perea, D. E.; Evans, J. E.; Lauhon, L. J.; Zhang, J.-G.; Liu, J.; Browning, N. D.; Cui, Y.; Arslan, Y.; Wang, C.-M. *Nano Lett.* **2013**, *13*, 6106−6112.
(202) Sacci, R. L.; Dudney, N. J.; More, K. L.; Parent, L. R.; Arslan, I.; Browning, N. D.; Unocic, R. R. *Chem. Commun.* **2014**, *50*, 2104−2107.
(203) Zeng, Z.; Liang, W.-I.; Liao, H.-G.; Xin, H. L.; Chu, Y.-H.; Zheng, H. *Nano Lett.* **2014**, *14*, 1745−1750.
(204) Holtz, M. E.; Yu, Y.; Gunceler, D.; Gao, J.; Sundararaman, R.; Schwarz, K. A.; Arias, T. A.; Abruña, H. D.; Muller, D. A. *Nano Lett.* **2014**, *14*, 1453−1459.
(205) Mehdi, B. L.; Gu, M.; Parent, L. R.; Xu, W.; Nasybulin, E. N.; Chen, X.; Unocic, R. R.; Xu, P.; Welch, D. A.; Abellan, P.; Zhang, J.-G.; Liu, J.; Wang, C.-M.; Arslan, I.; Evans, J.; Browning, N. D. *Microsc. Microanal.* **2014**, *20*, 484−492.
(206) Sacci, R. L.; Black, J. M.; Balke, N.; Dudney, N. J.; More, K. L.; Unocic, R. R. *Nano Lett.* **2015**, *15*, 2011−2018.
(207) Mehdi, B. L.; Qian, J.; Nasybulin, E.; Park, C.; Welch, D. A.; Faller, R.; Mehta, H.; Henderson, W. A.; Xu, W.; Wang, C. M.; Evans, J. E.; Liu, J.; Zhang, J.-G.; Mueller, K. T.; Browning, N. D. *Nano Lett.* **2015**, *15*, 2168−2173.
(208) Leenheer, A. J.; Jungjohann, K. L.; Zavadil, K. R.; Sullivan, J. P.; Harris, C. T. *ACS Nano* **2015**, *9*, 4379−4389.
(209) Williamson, M. J.; Tromp, R. M.; Vereecken, P. M.; Hull, R.; Ross, F. M. *Nat. Mater.* **2003**, *2*, 532−536.
(210) Chen, X.; Noh, K. W.; Wen, J. G.; Dillon, S. J. *Acta Mater.* **2012**, *60*, 192−198.
(211) White, E. R.; Singer, S. B.; Augustyn, V.; Hubbard, W. A.; Mecklenburg, M.; Dunn, B.; Regan, B. C. *ACS Nano* **2012**, *6*, 6308−6317.
(212) Liu, J.; Wei, B.; Sloppy, J. D.; Ouyang, L.; Ni, C.; Martin, D. C. *ACS Macro Lett.* **2015**, *4*, 897−900.
(213) Unocic, R. R.; Sacci, R. L.; Brown, G. M.; Veith, G. M.; Dudney, N. J.; More, K. L.; Walden, F. S.; Gardiner, D. S.; Damiano, J.; Nackashi, D. P. *Microsc. Microanal.* **2014**, *20*, 452−461.
(214) Welch, D. A.; Mehdi, B. L.; Hatchell, H. J.; Faller, R.; Evans, J. E.; Browning, N. D. *Adv. Struct. Chem. Imag.* **2015**, *1*, 1−11.

DOI: 10.1021/acs.analchem.5b04542
Anal. Chem. 2016, 88, 414−430